Swiss J Geosci (2015) 108:401–424
DOI 10.1007/s00015-015-0200-5

# Deciphering neotectonics from river profile analysis in the karst Jura Mountains (northern Alpine foreland)

**Mickael Rabin[1] · Christian Sue[1] · Pierre G. Valla[2] · Jean-Daniel Champagnac[3] · Nicolas Carry[1] · Vincent Bichet[1] · Urs Eichenberger[4] · Jacques Mudry[1]**

Received: 8 April 2015 / Accepted: 7 September 2015 / Published online: 16 October 2015


**Abstract** The study of the neotectonic activity in the Jura Mountains (northwestern most belt of the European Alps) represents a challenge in the application of quantitative geomorphology to extract landscape metrics and discuss potential coupling between tectonic, climatic and lithospheric mechanisms during the evolution of this mountain belt. The Jura Mountains are characterized by a karst calcareous bedrock, slightly affected by Quaternary glaciations, and by moderated uplift rates (<1 mm/year). In this study, we performed river profile analyses to decipher comparable geomorphological signals along tectonic structures within the entire Jura arc. Our results suggest higher tectonic activity in the High Range of the belt (internal part) than in the External Range, which is discussed in terms of deformation mechanisms. Integration of our results with previous geomorphological, neotectonic and geodetic studies from the literature leads us to propose new potential lithospheric and tectonic mechanism(s) driving the Plio-Quaternary deformation of the Jura Mountains. Our study finally reveals a regional-scale correlation between neotectonic deformations recorded by the Jura drainage network and the predicted isostatic rebound in response to Alpine Quaternary erosion. However, the correlation between our geomorphic signals and compressive structures suggests that the Jura Mountains could be still in horizontal shortening in both the High Range and the External Range.

**Keywords** Neotectonics · Geomorphology · River profile · Knickpoints · Karst · Structural patterns · Jura Mountains · Alps

Editorial handling: S. Schmid.

**Electronic supplementary material** The online version of this article (doi:10.1007/s00015-015-0200-5) contains supplementary material, which is available to authorized users.

✉ Mickael Rabin
mickael.rabin@univ-fcomte.fr

[1] CNRS-UMR 6249 Chrono-environnement, University of Franche-Comté, 25030 Besançon, France

[2] Institute of Earth Surface Dynamics, University of Lausanne, 1015 Lausanne, Switzerland

[3] Institute of Geology, ETH Zürich, 8092 Zurich, Switzerland

[4] ISSKA, 2301 La-Chaux-de-Fonds, Switzerland

## 1 Introduction

Quantifying the deformation and uplift rates of active mountain belts represents a major challenge in our understanding of the existing coupling between lithospheric mechanisms, tectonic activity and landscape evolution (Ruddiman et al. 1988; Molnar and England 1990; Molnar 2009; Whipple 2009; Champagnac et al. 2012). Moreover, quantification of the recent tectonic activity in slowly deforming mountainous environments remains challenging because deformation markers have been potentially modified or erased by climatically-driven surface processes over the Quaternary period (Whipple 2001; Carretier et al. 2006).

Mountainous landscapes are the complex result of interactions between tectonics, climatically driven erosion processes, geodynamic and lithospheric processes mechanisms, and, to a minor extent, anthropogenic activities. Since the end of the 1980s, geoscientists have been increasingly interested in the understanding, quantification, and modeling of the complex interactions between exhumation, tectonic and erosion processes (Ruddiman and Kutzbach 1989; Molnar and England 1990; LeMasurier and Landis 1996; Schlunegger and Hinderer 2003; Valla

et al. 2012; Fox et al. 2015). In this framework, numerous studies focused on river morphology to quantify the interplay between tectonics and fluvial erosion (e.g., Jackson et al. 1996; Demoulin 1998; Snyder et al. 2000; Kirby and Whipple 2001; Whipple 2004; Wobus et al. 2006; Sougnez and Vanacker 2010; Castelltort et al. 2012; Walsh et al. 2012). Indeed, river profiles are quantitative markers of endogenous/exogenous processes and may reveal neotectonic activity by changes induced in parameters such as concavity, steepness or hypsometric integral. Here, we consider the Jura belt in order to highlight potential neotectonic-related deformations using river profile analysis. The Jura Mountains, which are the most recent tectonic expression of the Alpine orogeny (Fig. 1) and have been less impacted than the Alps by the last glacial events, appear as a suitable setting for assessing neotectonic activity in the Alpine orogen.

The aim of this study is to identify and characterize neotectonically controlled disturbances along river profiles of the Jura Mountains. Thereby we combine morphometric and field observations in order to identify landscape markers pointing towards potential neotectonic activity. We also highlight potential methodological problems and complexity when using river profiles in limestone-bedrock settings, where karst groundwater flow is an important component of the hydrological system.

## 2 Overall framework

### 2.1 Geological and tectonic setting

#### *2.1.1 Structure and tectonic evolution of the Jura*

The Jura mountain belt is the most external and one of the most recent tectonic expressions of the Alpine orogeny (Fig. 1). Its southern tip merges with the front of the subalpine belt (Chaînes Subalpines, i.e., the Chartreuse Massif), while its northeastern part is separated from the Alps by the Molasse Basin. This basin is an Oligo-Miocene foredeep basin developed at the northern front of the European Alps (Rollier 1903; Heim 1919; Aubert 1949; Lebeau 1951; Lyon-Caen and Molnar 1989; Burkhard 1990; Pfiffner 1990; Henry et al. 1997; Schlunegger et al. 1997; Sommaruga 1999; Becker 2000; Laubscher 2010).

The Jura is surrounded to the west and the north by peri-alpine N–S oriented Tertiary rifts (Merle and Michon 2001; Dèzes et al. 2004); namely the Bresse Graben and the Rhine Graben, respectively (Fig. 1). Its northern boundary is affected by NNE-SSW to ENE-WSW normal faults associated to Tertiary rifting and corresponding to the Rhine-Bresse Transfer Zone (RBTZ) (Fig. 1) (Lacombe et al. 1993 and references therein; Madritsch et al. 2009). The Jura Mountains consist of Mesozoic and Cenozoic deformed sediments that were detached from the underlying Paleozoic basement (Fig. 2). These sediments are hardly deformed in the Molasse Basin whereas they acquired a typical fold-and-thrust structure westward in the Jura arc. They consist of Jurassic and Cretaceous marls and limestones detached along a basal décollement of Triassic evaporites. The Paleozoic basement is exposed beyond the northern front of the Jura (Serre massif, Fig. 1), and is composed of medium to high grade metamorphic and plutonic rocks deformed during the Variscan orogeny covered by Stephano-Permian sediments (Rollier 1903; Lyon-Caen and Molnar 1989; Mosar 1999; Coromina and Fabbri 2004; Laubscher 2010, Fig. 2).

The Jura belt is a typical thin-skinned fold-and-thrust belt (Laubscher 1992; Hindle 1997; Burkhard and Sommaruga 1998; Homberg et al. 1999; Becker 2000; Affolter and Gratier 2004, Fig. 2). Large parts of it correspond to an orogenic arc composed of narrow strained zones separated by hardly deformed plateaus. These deformed zones, the so-called "Jura Faisceaux", are affected by arc-parallel folds and thrusts corresponding to a horizontal, SSE-NNW directed shortening. Its overall structure can be resumed in three main regions: (i) the High Range in the internal part (eastward), which is separated from; (ii) the External Range to the west by; (iii) barely deformed plateaus in the central part (Fig. 1).

This structure is crosscut by coeval left-lateral transpressive faults (e.g., Vuache, Morez, and Pontarlier faults) (Fig. 1), which delineate individual tectonic blocks and damped part of the shortening (Laubscher 1992; Homberg et al. 1997; Becker 2000; Affolter and Gratier 2004). The northern and eastern parts of Jura are characterized by E–W to NE–SW directed fold axes and thrusts, and N–S trending left-lateral strike-slip faults; whereas in the southwestern part thrusts and fold axes have a main N–S orientation and strike-slip faults are NW–SE oriented (Fig. 1).

The typical stair-step shape of the Jura structure has been acquired during the latest stage of the Alpine orogeny, in Late Miocene and Early Pliocene times (Sommaruga 1999; Becker 2000; Affolter and Gratier 2004). Folding and thrusting took place between about 14 and 3.3 Ma according to stratigraphic and paleontological evidences (Becker 2000; Ustaszewski and Schmid 2006, 2007 and references therein). However, geomorphological evidence suggest that more recent deformations (i.e., Pleistocene to Holocene) occured along the northernmost frontal thrusts of the Jura (Nivière and Winter 2000; Giamboni et al. 2004b; Carretier et al. 2006; Nivière et al. 2006; Ustaszewski and Schmid 2006, 2007; Madritsch et al. 2010b; Molliex et al. 2011). These authors highlight a Plio-Pleistocene N–S horizontal shortening in the external part of the Jura with an average uplift velocity of $\sim$0.05 mm/year at the front.

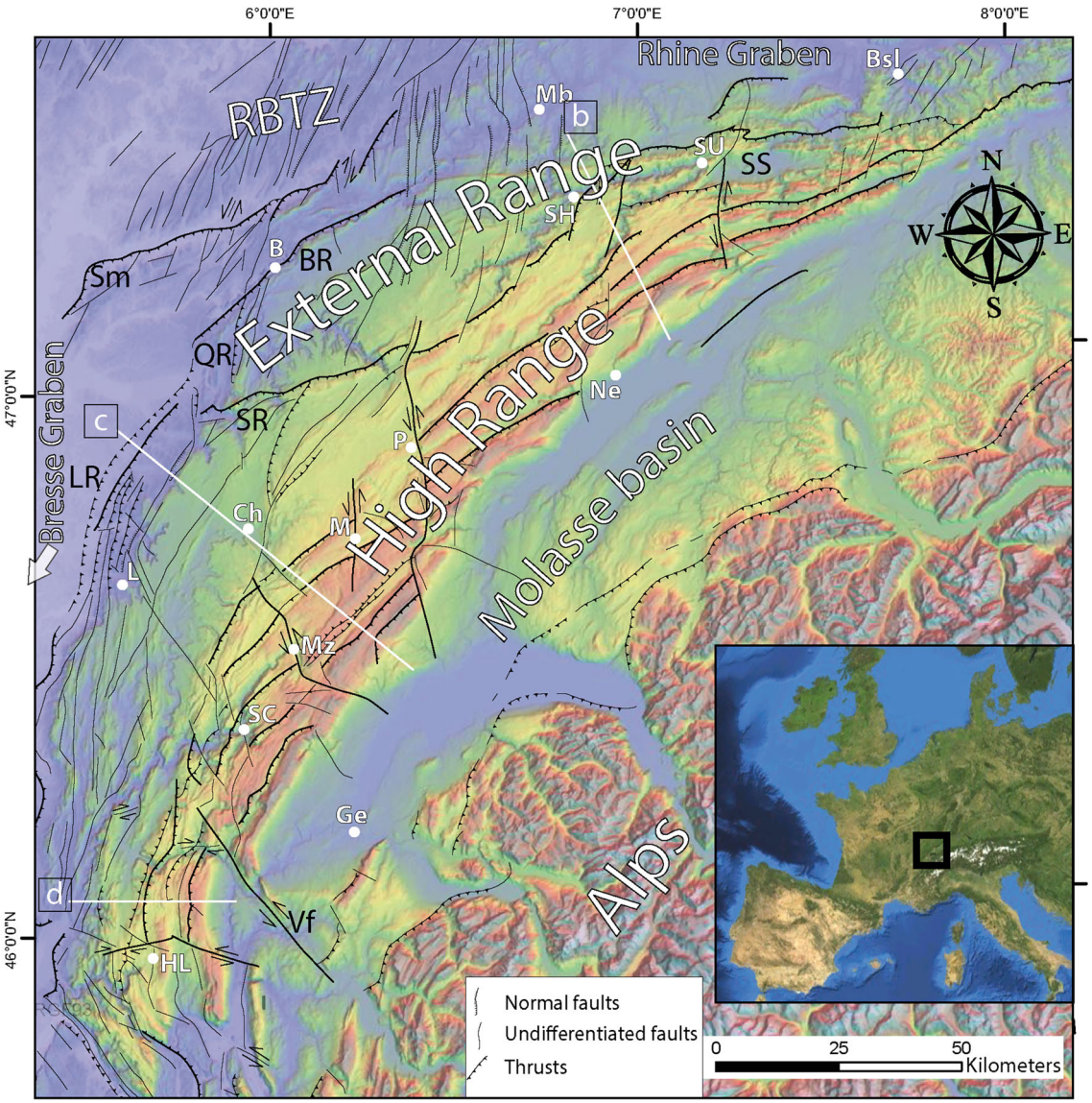


**Fig. 1** Simplified structural map of the Jura Mountains based on the BRGM geological map. City locations and structural regions are represented by *white* and *black letters*, respectively (*Bsl* Basel, *B* Besançon, *Ch* Champagnole, *Ge* Geneva, *HL* Hautevillle-Lompnes, *L* Lons-le-Saunier, *Mb* Montbéliard, *Mz* Morez, *M* Mouthe, *Ne* Neuchatel, *P* Pontarlier, *SC* Saint-Claude, *SH* Saint-Hippolyte, *Su* Saint-Ursanne; *Sm* Serre massif, *BR* Besançon Range, *LR* Lons Range, *QR* Quingey Range, *SR* Salins Range, *SS* Sorne Syncline, *Vf* Vuache fault). *Inset* shows location of the study area within western Europe

In summary, the Jura structure results from the succession of three main periods: (i) an Oligocene extension which results in the Bresse and Rhine Grabens and in few minor offset normal faults in the Jura Faisceaux (Homberg et al. 2002; Affolter and Gratier 2004 and references therein), while the implication of the Paleozoic basement in this phase is still discussed (Hindle1997; Homberg et al. 2002; Affolter and Gratier 2004); (ii) a N–S to NW–SE oriented shortening during the Late Miocene, resulting in the present fold and thrust structures (Hindle 1997; Affolter and Gratier 2004). Inherited structures from both the Variscan basement deformation and Oligocene cover extension could have, at least partly, controlled the geometry and the distribution of thrusts during this shortening phase (Hindle 1997; Homberg et al. 2002; Affolter and Gratier 2004 and references therein; Ustaszewski and Schmid 2006); and (iii) a Plio-Pleistocene northward propagation of shortening, which remains debated at present (Nivière and Winter 2000; Giamboni et al. 2004a; Ustaszewski and Schmid 2006). Based on surface in situ stress data (Becker 2000), deep seismicity distribution (e.g., Lacombe and Mouthereau 2002) and evidence of frontal basement-rooted fault reactivation (Ustaszewski and Schmid 2006, 2007; Madritsch et al. 2009), several authors have suggested a

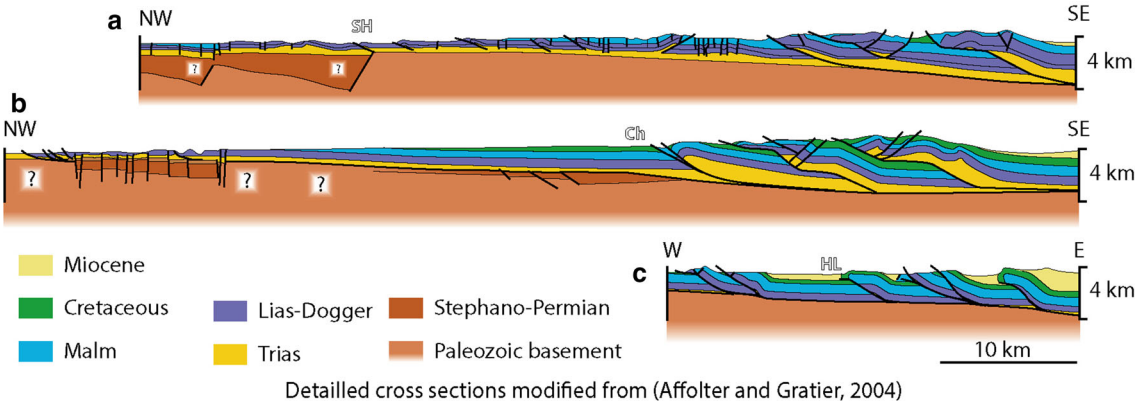


**Fig. 2** Schematic cross sections (modified after Affolter and Gratier 2004) approximatively relocated in Fig. 1 (*white lines*, see Sect. 2.1 for further details). *Question marks* on cross sections represent uncertainties on the deep geometry of the basement

change deformation style within the Jura during the Pliocene from a thin-skinned belt towards a thick-skinned belt. This could explain the northward propagation of shortening beyond the presence of the Triassic evaporites forming the main detachement of the thin-skinned Jura Mountains (e.g., Becker 2000; Ustaszewski and Schmid 2007; Madritsch et al. 2009).

### 2.1.2 *Recent deformation in the Jura Mountains*

The structure of the Jura has long been studied (Rollier 1903; Laubscher 1992; Hindle 1997; Burkhard and Sommaruga 1998; Homberg et al. 1999; Becker 2000; Nivière and Winter 2000; Affolter and Gratier 2004), but its recent to modern tectonic activity still remains a matter of debate. Neotectonic activity and recent uplift history of the Jura have been studied using different geophysical and geomorphological approaches (Jouanne et al. 1995, 1998; Nivière and Winter 2000; Nocquet and Calais 2003; Giamboni et al. 2004b; Walpersdorf et al. 2006; Madritsch et al. 2010a, b). Jouanne et al. (1995, 1998), Nivière and Winter (2000) and Nivière et al. (2006) have shown a northward propagation of thin-skinned deformation style with uplift rates of $\sim$0.7 mm/year from leveling data in the internal part of the southern Jura (Jouanne et al. 1998) and a long-term mean uplift velocity of $\sim$0.3 mm/year along the northernmost frontal thrust (Nivière et al. 2006). This propagation of shortening is estimated with horizontal velocities of 3–4 mm/year using GPS data (Jouanne et al. 1998). However, recent geodetic studies based on GPS network analysis reveal horizontal velocities lower than 1 mm/year (Nocquet and Calais 2003; Walpersdorf et al. 2006) associated with a main strain feature in favor of an arc-parallel extension. Moreover, geomorphological evidence of fold growth suggests a long-term mean uplift velocity of only $\sim$0.05 mm/year along the External Range, associated with a thick-skinned deformation mode (Giamboni et al. 2004b; Ustaszewski and Schmid 2007; Madritsch et al. 2010a; Molliex et al. 2011).

It thus appears that GPS data available in the Jura Mountains bear witness of disagreement between different studies (Jouanne et al. 1998; Schlatter et al. 2005; Walpersdorf et al. 2006), interpretations varying from ongoing uplifting belt (Jouanne et al. 1998) to arc-parallel extension with very slow horizontal movements (Walpersdorf et al. 2006). Considering the hypothesis of ongoing horizontal shortening, there is a debate about both the actual deformation style (thin- vs thick-skinned) and the long-term mean uplift rates (from 0.05 to 0.3 mm/year, e.g., Nivière et al. 2006; Madritsch et al. 2010a).

Moreover, the neotectonic activity in the Jura Mountains is also discussed in terms of deformation style, based on the seismic data and focal mechanisms. Indeed, Lacombe and Mouthereau (2002) noted that the majority of earthquakes recorded in the Jura Mountains are distributed throughout the entire crust (down to 30 km depth, with a higher density around 15–20 km depth), that is to say under the brittle-ductile transition. These crustal earthquakes have been associated to the presence of high-pressure fluids which allow brittle failure to occur at such important depths (Deichmann 1992). This argues for a present-day activity in the basement under the Jura cover and has been interpreted as evidence for ongoing shortening in a thick-skinned mode (Lacombe and Mouthereau 2002). Nevertheless, the general synthesis of earthquakes occurring in the Jura and the northern Alps proposed by Kastrup et al. (2004) has shown that most earthquakes in the Jura belt have strike-slip focal mechanisms. Moreover, the majority of recorded earthquakes are located in the northwestern Jura with focal mechanisms associated with WNW-SSE steep faults (e.g., Lacombe and Mouthereau 2002; Kastrup et al. 2004) which is not in agreement with the orientations of the inherited Variscan faults (Hindle 1997; Homberg et al. 2002; Affolter and Gratier 2004 and references

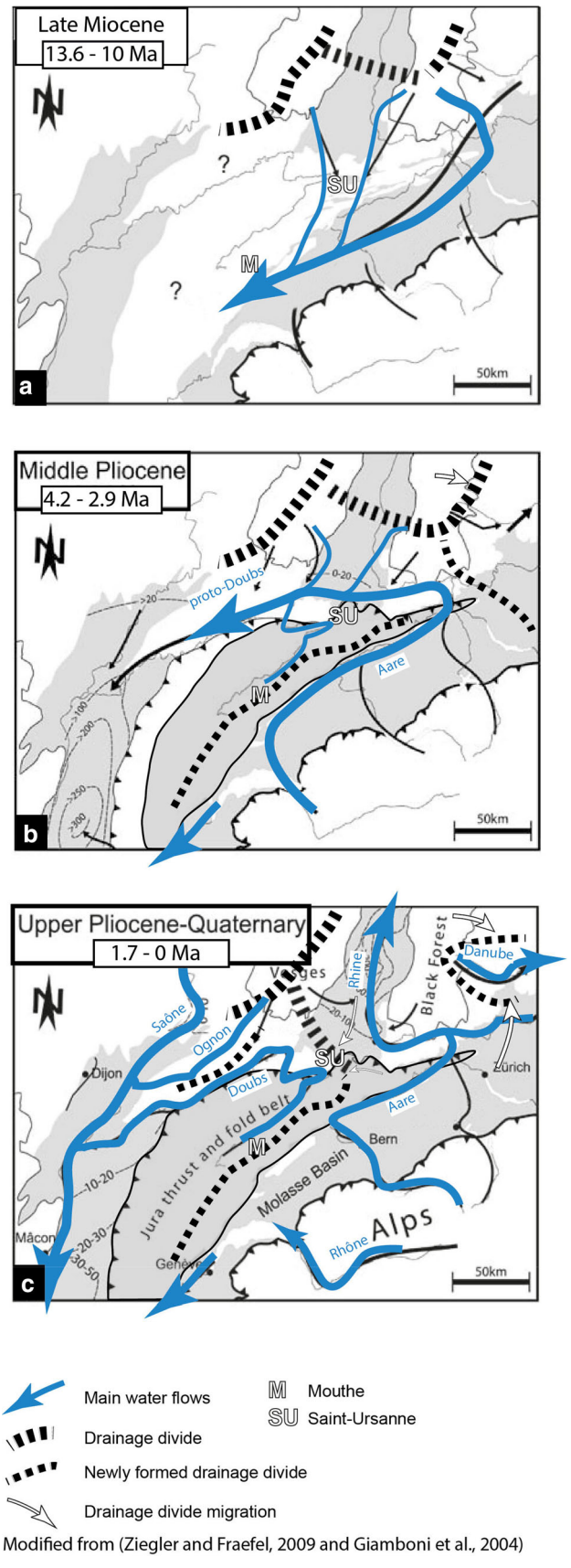


**Fig. 3** Schematic map of the northern Alpine river network organization from the Late Miocene (13.6–10 Ma) to present-day, modified from Ziegler and Fraefel (2009) and Giamboni et al. (2004a, b). **a** the entire Alpine foreland drained southwestward during the Late Miocene; **b** northeast deflection of the Swiss Molasse river network in response to the incipient Jura folding; **c** capture of a part of the Doubs, Danube and Rhine rivers in response of Upper Rhine Graben subsidence, and karst interactions (see Sect. 2.1.2 for further details)

therein; Ustaszewski and Schmid 2006). However, the relatively poor resolution on focal depth, together with the absence of lower crustal events in the southwestern Jura, does not allow providing a clear interpretation towards an ongoing thick-skinned activity within the overall Jura Mountains.

Beyond the mode of deformation in the Jura arc, the traditionally accepted model of an active collisional activity for the Jura, in dynamic continuity with the Alps, rises the issue of its geodynamic origin. The European Alps are in a post-collisional regime (Champagnac et al. 2009; Sue et al. 2007; Nocquet 2012; Valla et al. 2012), and are characterized by isostatic-related extension and uplift, due to the interaction between buoyancy forces and erosional dynamics (Sue et al. 1999; Champagnac et al. 2007; Sue et al. 2007; Delacou et al. 2008; Serpelloni et al. 2013; Vernant et al. 2013; Baran et al. 2014).

## 2.2 Hydrogeological setting

The arc shaped area of the Jura Mountains of about 15,000 km$^2$ is characterized by a strong karst imprint. Currently, this region is under semi-continental climate influence with mean annual precipitations rates of 1000–2000 mm/year with no significant spatial patterns across the belt (Frei and Schar 1998; Calmels et al. 2014).

The present-day Jura drainage network is complex and results from a multi-step evolution controlled by tectonic events and karst processes. Prior to the Jura shortening and uplift, the regional drainage network was flowing over the entire Alpine foreland (i.e., south of the Vosges, Fig. 3a) and drained southwestward during the Miocene times (~13.5–10 Ma; Giamboni et al. 2004a; Ziegler and Fraefel 2009). This palaeodrainage network is important for understanding both the growth of the Jura arc and the present-day drainage network. First folds appeared in the Late Miocene during a first shortening phase and were restricted to the internal part. The newly formed internal massif separated the former drainage network in two distinct parts: (i) the Molasse Basin rivers, which have been partly deflected to the northeast (the Aare-Doubs River, Fig. 3b); and (ii) new rivers in the High Range (e.g., the Doubs River). The southwestern part of the internal area (between the first Jura folds and the Alpine front), was

most probably already drained by the Rhône River towards the southwest (Denizot 1952; Mocochain et al. 2006).

The northern side of the proto-Jura was drained by a new river network flowing northeastward, corresponding to the present-day Doubs River in its upstream part (from Mouthe to Saint-Ursanne, Figs. 1, 3). The Doubs River in this region is a subsequent river (i.e., adapted to the structural patterns), following synclines axes and cross-cutting anticlines using transverse faults or low points along the anticline axis in order to join a lower syncline westward (Fournier 1900; Gibert 1945; Ziegler and Fraefel 2009).

During the northwestward propagation of the Jura deformation in the Plio-Pleistocene (Madritsch et al. 2010b; Molliex et al. 2011), the former southwestward-flowing network maintained its initial course, corresponding to the present-day downstream part of the Doubs River (from Montbéliard to its outlet, see Figs. 1, 3c). In this region, the Doubs River is antecedent to the late frontal folds (Giamboni et al. 2004a; Ziegler and Fraefel 2009) but sedimentary analysis had revealed that the Ognon and the Doubs Rivers were never connected (Fig. 3b), suggesting that a previous topographic high existed before the proto-Doubs River development (Late Miocene to Early Pliocene; Madritsch et al. 2012).

The link between the upper Doubs River (upstream of Saint-Ursanne, corresponding to a subsequent network coeval with the beginning of folding), and its downstream part (from Montbéliard to its mouth, which corresponds to an antecedent southwestward network), could result from the Rhine Graben subsidence (Ziegler and Fraefel 2009) associated with the folding of the frontal range and/or from a karst capture of the upstream part by a tributary of the northernmost network (Fournier 1900; Gibert 1945). This would explain the present-day half-turn of the Doubs River observed near Saint-Ursanne (Fig. 3c).

In the intermediate Jura plateaus (WNW of Pontarlier and Champagnole area, Fig. 1), the drainage network is mainly karstic and organized in a complex underground system. The southern part of these plateaus is drained by the Ain River which is fed by both karst springs and surface drainage networks. This river flows southwestward and seems acting like a subsequent river. The Loue River, farther north, drains the northern part of the plateau and is mainly fed by the uppermost part of the Doubs River via a karst spring (Fig. 4).

The present-day rivers flow mainly parallel to structural axes in the folded areas (Fig. 4). This river network consists in six main rivers: the Doubs, Ain, Loue, Aare, Rhine and Rhône rivers (Fig. 4). Aare, Rhine and Rhône rivers mainly flow through the Alpine area before flowing across the Jura and carry alpine sediments, which modifies their erosive power (Golterman 1982; Kühni and Pfiffner 2001; Preusser and Schlüchter 2004). For this reason, these rivers cannot be easily compared with Jura rivers *sensus stricto*, neither regarding erosivity nor water regime. In the following we will focus only on rivers having their sources in the Jura Mountains.

### 2.3 Glacial setting

Similar to the European Alps, the Jura Mountains have been affected by Quaternary glaciations (Campy 1992; Buoncristiani and Campy 2004a, b). In the Jura, evidence of the two last glacial maxima have already been described (Campy 1982). The older maximum is known as the Riss period and dated at around 130 ka (Ostermann et al. 2006). During this period, the central part of the Jura Mountains was completely covered by ice (up to ~600-m thick in the High Range), distinct from the Alpine glaciers (Campy 1992; Buoncristiani and Campy 2004a; Coutterand 2010) (Fig. 5a). The Jura Mountains have also been glaciated during the Würm period [i.e., Last Glacial Maximum from ~21 ka to 17 ka (Buoncristiani and Campy 2004b; Coutterand 2010)] (Fig. 5b) although the ice-cap was ~200 m thinner and less extended toward the NW than during the Riss glaciation (Campy 1992).

During these glacial periods, the Jura glacier was partly disconnected from Alpine glaciers (Buoncristiani and Campy 2004a), thus erosion and sediment transport was limited into transversal valleys and on the Jura plateaus (Campy 1985, 1992). The Jura Mountains represent a total surface of about 15,400 $km^2$, a glacier covering a surface inferior to 50,000 $km^2$ (like in the Jura case) and having a dome shape (Campy 1985, 1992) (Fig. 5) is called an ice-cap after the National Snow and Ice Data Center (http://nsidc.org). Ice caps, such as the Jura one, have particular erosion dynamics localized at ice margins (Kleman 1994; Golledge et al. 2009; Thomson et al. 2010), where meltwater flows under the ice and is limited to a relatively thin corona behind the frontal moraines. Moreover, based on peripheral glacial sediment accumulation, Buoncristiani and Campy (2001) estimated a relatively high erosion rate of ~1.6 mm/year between ~21 and 17 ka.

Within formerly glaciated areas, rivers of the more internal and southern parts of the present-day Jura Mountains partly flow in glacial sediments (e.g., Ain River, Fig. 4) and have been impacted by glacial erosion with potential erasing of geomorphological markers along their profile. As a consequence, we can assume that the present-day longitudinal profiles of the Jura rivers in these parts have recorded potential tectonic activity only since ~17 ka, i.e., since the last ice retreat (Campy 1992; Buoncristiani and Campy 2004a, b).

During Quaternary times, the northern half of the Jura Mountains stayed outside the ice cap (Campy 1992; Buoncristiani and Campy 2004a), and studies carried out

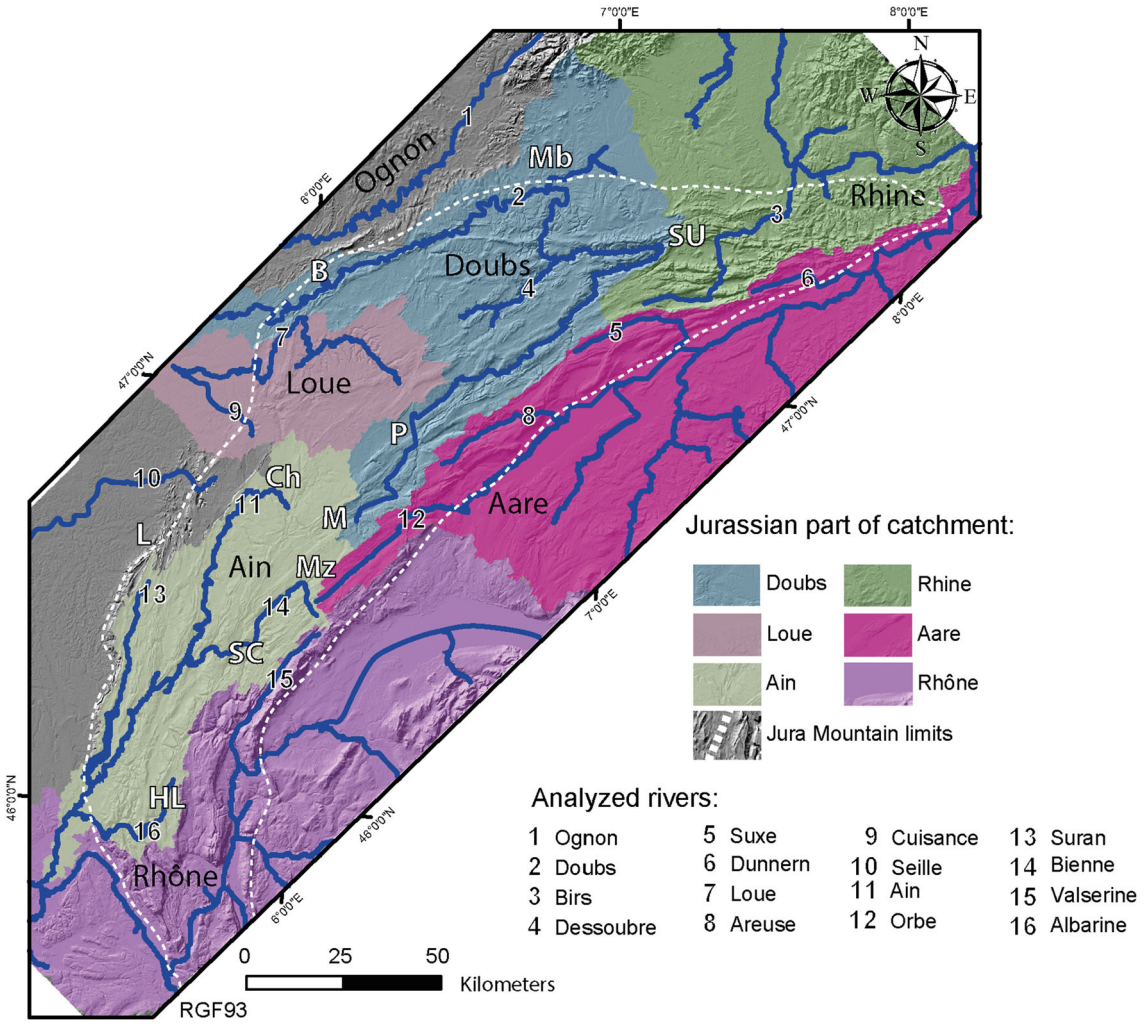


**Fig. 4** Map of main river catchments in the Jura Mountains (Doubs, Ain, Loue, Aare, Rhine, Rhône). The sixteen analyzed rivers are also indicated (*numbers 1–16*), and the morphological limits of the Jura Mountains are represented by the *white dotted line*

on glacial and alluvial deposits in these areas indicate that the main part of the present-day river network was already organized before late-Pleistocene glaciations (Campy 1985; Campy et al. 1994; Bichet et al. 1999; Buoncristiani and Campy 2004b; Giamboni et al. 2004a; Ziegler and Fraefel 2009). Recent evidence from the northeastern part of the Jura Mountains shows that Quaternary climate changes had no significant effect on the tectonic imprint recorded by river profiles in the Jura context (Carretier et al. 2006). This implies spatially-uniform erosion processes in this region, which we assumed to be similar in the formerly-glaciated parts of the Jura since deglaciation. Under these conditions, modern rivers are expected to preserve topographic anomalies caused by uplift variations over about tens of thousands of years (e.g., Whipple and Tucker 1999; Carretier et al. 2006). In turn, the river profile analysis could help us to constrain neotectonic activity in the Jura arc since the late glacial period.

## 3 Methodology

### 3.1 Theoretical framework

Quantitative morphotectonic approaches have been increasingly used to infer the interactions between climate and tectonics in landscape evolution (Kühni and Pfiffner 2001; van der Beek and Bourbon 2008; Champagnac et al. 2012; Vernant et al. 2013; Steer et al. 2014). Amongst those river profile analyses following the stream power model have been widely used to quantify the degree and the nature of potential disequilibrium between the tectonic forcing and the fluvial erosional agent (e.g., Campbell 1964; Snyder et al. 2000; Kirby and Whipple 2001; Goldrick and Bishop 2007; Shahzad et al. 2007; Robl et al. 2008; Rantitsch et al. 2009; DiBiase et al. 2010; Phillips et al. 2010; Singh and Awasthi 2010; Walsh et al. 2012). Based on the stream power model and under steady-state

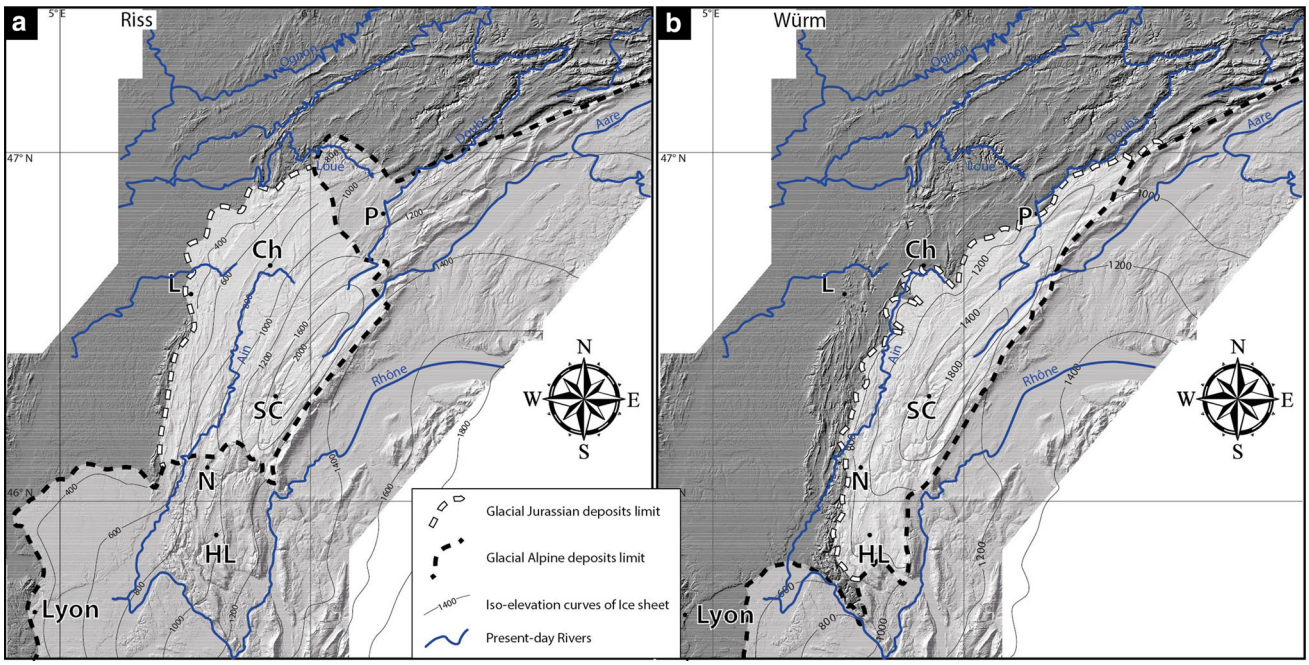


**Fig. 5** Ice extent over the Jura Mountains during the two last glacial periods (Riss and Würm, modified from Campy 1992; Buoncristiani and Campy 2004a). The Jura ice cap is represented by the *white shaded area*, and the Alpine glaciers by the *light grey shaded area*. **a** Ice extent during the Riss glacial period (~130 ka). The Jura has developed its own ice cap, disconnected from Alpine glaciers. This period is the most extensive glacial event in the Jura Mountains. **b** Ice extent during the late Würm (25–17 ka), showing a significantly smaller Jura ice cap than during the Riss (see Sect. 2.3 for further details). *Black letters* represent the city locations with the same legend as in Fig. 1

conditions (i.e., bedrock erosion equals uplift rate), river slope profiles (S) can be theoretically derived following the equation (Whipple and Tucker 1999, for more details, see the Appendix 1 in the supplementary material).

$$S = k_s \cdot A^{-\theta} \quad (1)$$

where $k_s$ sets the channel steepness, A is the drained area and θ is the intrinsic channel concavity (Whipple and Tucker 1999; Kirby and Whipple 2001; Whipple 2004; Wobus et al. 2006; Croissant and Braun 2014).

Comparison between this theoretical profile under steady-state conditions and the observed longitudinal profile can highlight potential anomalies along the river. These anomalies may depend on either lithological contrasts, local changes in the water regime and/or spatio-temporal changes in uplift rates or climatic forcing (Willgoose et al. 1991a, b; Howard 1994; Whipple and Tucker 1999).

In this framework, the comparison of an observed river profile with the theoretical prediction (Eq. 1) can highlight potential local slope variations called hereafter knickpoint(s) or knickzone(s) (Whipple and Tucker 1999). These can be explained either by spatial variations in the drainage area A or in the channel steepness $k_s$. A knickzone has been defined as "a convex up and steep segment of the river consisting of an increasing steepness transition, steepness maximum, and decreasing steepness transition" (e.g., Whipple and Tucker 1999; Walsh et al. 2012). In the present study, we localized the knickpoint at the maximum steepness locus (see for instance graphs shown in Appendix 4 of the supplementary material).

Under uniform erosion processes, variations in $k_s$ could evidence spatial or temporal variations in the rock uplift (tectonic) forcing (Whipple and Tucker 1999). The temperate climate and uniform distribution of rainfall in the Jura Mountains allows us to assume rather spatially-uniform erosion processes since the LGM. However, lithological, karstic and anthropogenic perturbations along the river profile may also induce local slope variations, resulting in spatial variations in the channel steepness $k_s$ (e.g., Sternai et al. 2012; Walsh et al. 2012).

## 3.2 River profile analysis

### *3.2.1 River profile extraction and knickpoint identification*

Longitudinal profiles of 16 rivers have been analyzed within the Jura Mountains (Fig. 4). Their sources are all localized in the Jura arc and the main (or entire) part of their drainage areas is enclosed within the Jura Mountains. Five of these rivers mainly flow only through the High Range (rivers 6, 5, 8, 12 and 15 on Fig. 4), three rivers flow through the intermediate plateaus and the External Range

(rivers 4, 7 and 11 on Fig. 4), and four only flow through the External Range (rivers 1, 9, 10 and 13 on Fig. 4). The four last rivers flow both in the High and External Ranges (rivers 2, 3, 14 and 16 on Fig. 4), while the Doubs River (river 2) also flows through the intermediate plateaus. River longitudinal profiles have been analyzed following the protocol summarized hereafter (see Appendix 1 in the supplementary material for further details).

Catchment boundaries and river longitudinal profiles have been extracted from a compilation of a 25-m resolution digital elevation model (DEM) from the IGN (French *Institut de Geographie National*) and a 30-m resolution ASTER DEM from the NASA using the ArcGIS 10.1© platform. The vertical precision of the DEM is spatially heterogeneous and is around 2–3 m. Watershed extraction, river network and topographic slope rasters have been calculated with archydrotools (ESRI) and Stream Profiler toolbar (Whipple et al. 2007) on the ArcGis 10.1© platform.

Profile extraction has been performed with Stream Profiler code of Whipple et al. (2007) on Matlab R2012a©. Since neotectonic deformations in the Jura Mountains are expected to be of low magnitude (<1 mm/year, see Sect. 2.1.2 for details), it is important to evaluate the DEM data in terms of quality and resolution. For this purpose, and after several tests, we decided to perform our river profile analyses on unsmoothed DEM data (see for instance Whipple et al. 2007).

Because of the very noisy slope-area graphs we obtained (see Appendix 2 in the supplementary material), the classic approach of dividing the river profiles into different segments (Whipple 2004; Walsh et al. 2012) could not be adopted in our case; so we have decided to assess $k_s$ variations all along the river profile using the integral method described in Kirby and Whipple (2012 and references therein). This method allows defining a normalized $k_s$ from drainage area only, without using the log–log slope area graphs. This normalization also allows us to compare our results for different rivers, following:

$$z(x) = k_{sn} \int_0^x A(x')^{-\theta} dx' \equiv k_{sn} \chi(x) \quad (2)$$

where z is the elevation and x is the distance downstream. $\chi(x) = \int_0^x A(x')^{-\theta} dx'$ corresponds to the area beyond $A = f(x)$ and $k_{sn}$ was calculated over a 500-m sliding window using a reference concavity ($\theta_{ref} = 0.45$, Kirby and Whipple 2012) and using a channel spatial resolution of 250 m.

Since the structural pattern of the Jura Mountains has been relatively well described and mapped (Fig. 1), knickpoints have been discriminated individually rather than mapping long-wavelength changes in river slope. This allows us to directly compare their spatial correlations with the structural patterns (i.e., mapped faults, thrusts, folds) and to eventually discuss the potential tectonic mechanisms at their origin.

In this framework, and to keep our results comparable within the different studied rivers, we arbitrarily fixed a $k_{sn}$ threshold at the 80$^{th}$ percentile of $k_{sn}$ values on each individual river in order to keep that threshold adjusted to the water regime of each river. This approach allows discriminating even small $k_{sn}$ variations that we associate to individual knickpoints or knickzones. Following that approach, we looked for numerous but very sensitive signals induced by very little disturbances along the river profiles. The locations of these geomorphic signals have been subsequently evaluated by comparison with topographic, geological and hydrological maps.

### 3.2.2 *Factors inducing knickpoints*

Different factors can induce a knickpoint along a river profile, as already presented and discussed in many studies (e.g., Phillips et al. 2010; Walsh et al. 2012; Willett et al. 2014). Here, we paid particular attention on the discrimination of the different factors potentially controlling our observed knickpoints, as described thereafter.

Anthropogenic buildings such as dams or impoundments could disturb a river along its longitudinal profile. The impact of dams, both on the upstream and downstream parts of a river profile, is strongly depending on numerous factors such as dam location, local slope, environment, substrate nature, hydrological regime, or the availability of sediments. In general, the main disturbances occur downstream of a dam and are mainly controlled by variations of the sedimentary load (e.g., Kondolf 1997; Brandt 2000). It is difficult to predict the amplitude of these disturbances, the size of the affected zone or the time period needed by the river to re-equilibrate. However, Brandt (2000) stated that the river profile may have reached its previous state (i.e., before the dam construction) after only a few years, and the influence on the river geomorphology is slightly lowered if the impounded drainage area represents less than 35–40 % of the total drainage area of the river. Moreover, it seems that these disturbances are located near the dam and generally affect a length inferior or equal to ~20 times the river width (Brandt 2000 and references therein). To discard these potential biases, our river profile anomalies have been critically compared with the spatial locations of these anthropogenic features from topographic maps (IGN and Swisstopo, 1/25,000$^e$) and aerial photographs and field observations.

In the Jura Mountains, karst imprint is ubiquitous. The underground water networks are very complex and could connect several drainage basins together. Karst groundwater disturbs the river discharge at localized points such as seepages or karst outlets (see the example of the Loue

River in Appendix 3, supplementary material). Several Jura rivers are fed, at least partly, by karst springs. These karst features have been mapped using hydrological tracer tests from the DREAL Franche-Comté (Direction Régionale de l'Environnement, de l'Aménagement et du Logement, France) and from the OFEV (Office Fédéral de l'Environnement, Switzerland). One of the most obvious consequences of these karst connections is the capture of a river section, which could induce dramatic changes in the drainage organization (Mudry and Rosenthal 1977; Yanites et al. 2013). These events require several millions of years to be completed and the re-equilibration timescale of a river after a karst capture has been estimated in the Jura Mountains to about 1 Ma (Yanites et al. 2013). The half-turn shape of the Doubs River near Saint-Ursanne (Fig. 4) could result from such a karst capture (Fournier 1900; Gibert 1945) occurring during Pliocene times (Ziegler and Fraefel 2009). Another capture feature appears in the High Range (north of Mouthe, Fig. 4, see also Appendix 3 in the supplementary material) where the Doubs River is connected to the Loue River by a karst system (Mudry and Rosenthal 1977). This underground system is completely flooded and eroding, so it is possible that the Loue River will capture the upstream part of the Doubs in the future.

Lithological changes could also induce knickpoints by locally modifying bedrock erodibility (e.g., Walsh et al. 2012 and references therein). This potential influence has been carefully checked by comparing knickpoint locations and mapped lithological contrasts from detailed geological maps (1/50000[e] and 1/25,000[e], BRGM and Swisstopo). A particular attention has also been paid to geomorphological features such as landslides, rockslides or particular sedimentation patterns (alluvial fan, moraine deposits…) using aerial and field photographs.

After carefully checking and discarding all the potential non-tectonic controlling factors for river profile disturbances we selected the remaining neotectonically controlled knickpoints induced by tectonic structures such as thrusts, normal faults or folds that can induce a vertical displacement. Structures potentially inducing a change in the river path, such as a local slope change due to a pinched syncline or horizontal movement constraining the river to change its path, have also been considered.

Several factors may co-exist at the same location and their geomorphologic expressions will overprint each other. An identified knickpoint has not been interpreted as having a neotectonic control if at least one other factor was identified in its vicinity. Our results obtained from the 16 river profiles have been interpreted in terms of anthropogenic, lithological, karst or neotectonic forcing. We reported these results along the river profiles with their $k_{sn}$ evolution (see Appendix 4 in the supplementary material) and on georeferenced maps.

## 4 Results

Sixteen river profiles have been analyzed across the Jura Mountains (Fig. 4). The geometry of their longitudinal profiles is mainly controlled by the presence of karst outlets and dams (see Appendix 2 and 3 for further details, supplementary material). In the following, detailed results are presented for the three main and characteristic Jura rivers: (i) the Doubs River as an example of a river profile disturbed by complex structural patterns; (ii) the Ain River, an example of a river highly affected by human activity; and (iii) the Loue River as an illustration of a karst-controlled river. Only the most relevant knickpoints are detailed in the following. Full results on the 16 rivers can be found in the Appendix 4 of the supplementary material.

### 4.1 The Doubs River: a neotectonically-controlled river profile

The Doubs River represents the longest flow path within the Jura Mountains (450-km long), starting in the High Range where it follows structural axes before flowing through the intermediate plateaus and finally crossing the External Range before exiting the Jura. This river is therefore an excellent case study to highlight structural/neotectonics disturbances along its longitudinal profile.

The Doubs River starts with a karst spring in the High Range (Mouthe, Figs. 1, 4) and flows northeastward to Saint-Ursanne where it changes its flow direction to turn towards the west/southwest (Fig. 6). This river can be subdivided into three different sections: (i) the upstream part of the Doubs, corresponding to a subsequent river (i.e., adapted to the structural patterns); (ii) the segment between Saint-Ursanne and Montbéliard; (iii) the downstream segment from Montbéliard, meandering and acting as an antecedent river on structures (i.e., not adapted to structural patterns), which could be related to an old river network fed by the Vosges Massif and flowing southwestward before the Jura folding (Ziegler and Fraefel 2009, see Sect. 2.1.2 for details). The change in flow-direction near Saint-Ursanne has been proposed to have resulted from karst phenomena, possibly due to a capture of an ancient Doubs (Fournier 1900; Gibert 1945). This capture was potentially helped by the development of a N20°E oriented fold-thrust which now acts as a topographic barrier (SE of Saint-Ursanne, Fig. 6). After this capture, the spring of the Mouthe river became the main source of the Doubs River, resulting in the present-day flow path (Figs. 4, 6).

The first Doubs section shows seven knickpoints that appear to be strongly correlated with the structural pattern (knickpoint numbers 3, 4, 5, 10, 11, 12 and 13 on Fig. 6). Five of them correspond to anthropogenic disturbances

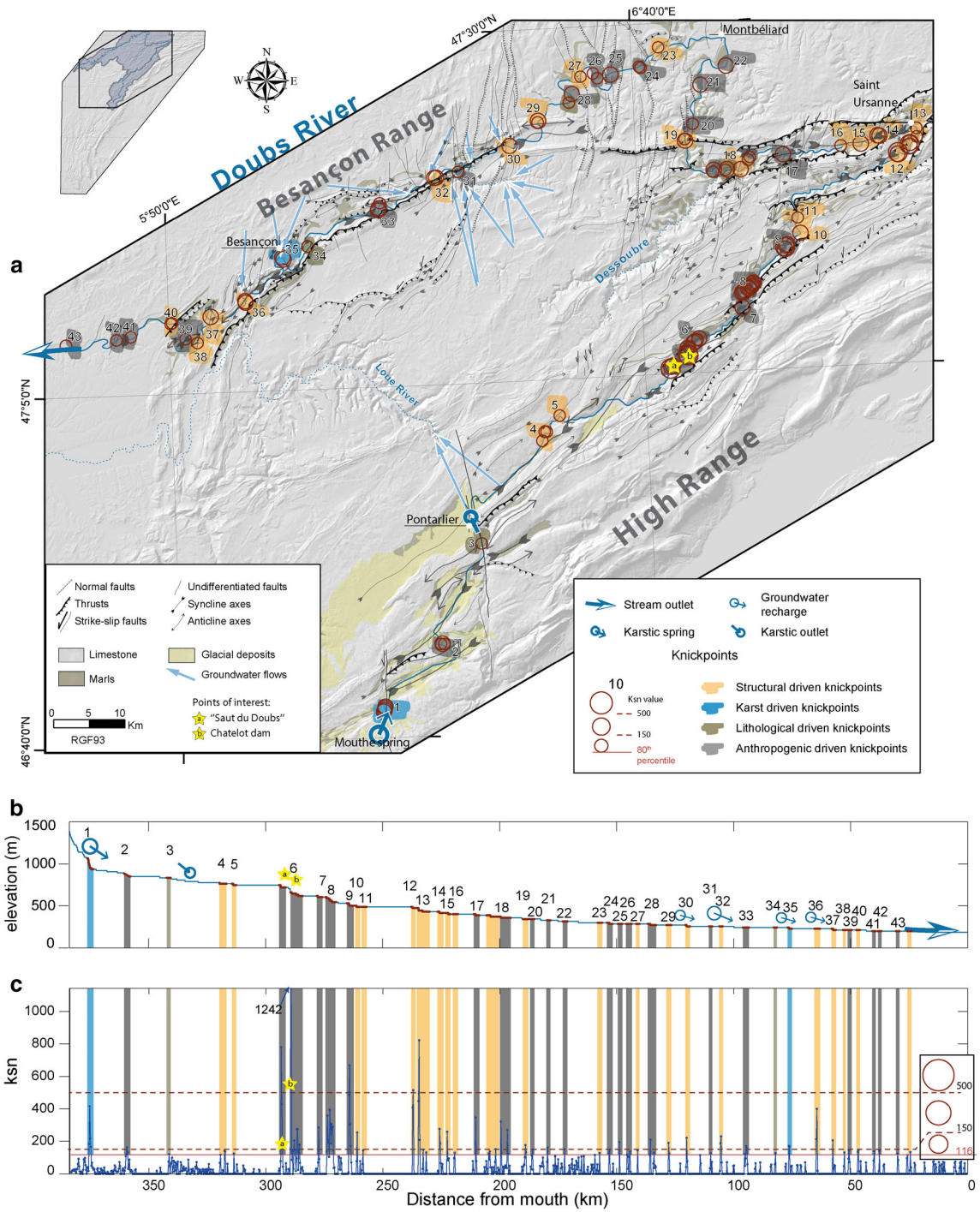


**Fig. 6** Map of the Doubs River (**a**), and its longitudinal profile (**b**) and $k_{sn}$ evolution (**c**). Lithological, karst and structural details have been reported along the Doubs path. Knickpoints (*red circles*) have been located and classified in size by their intensities ($k_{sn}$ values). Each knickzone has been interpreted regarding geological map of the BRGM (http://editions.brgm.fr/cartegeol.jsp) and from Swisstopo (http://www.swisstopo.admin.ch/internet/swisstopo/fr/home/products/maps.html), topographic maps from IGN (http://www.ign.fr) and Swisstopo, and hydrological maps from the OFEV (http://www.bafu.admin.ch) and the DREAL (http://carmen.application.developpement-durable.gouv.fr/14/CarteInfo.map) in term of potential lithological, structural (tectonic), anthropogenic, and karst forcing (for color code, see legend). See Sects. 2.1.2 and 4.1 for further details

(knickpoint numbers 2, 6, 7, 8 and 9) and only one from karst origin (knickpoint number 1 linked to the karst spring of the Doubs, Fig. 6). At this specific location, the discharge of the Doubs is completely disconnected from surface runoffs and is strongly controlled by the groundwater network that crosses structures and does not follow

valley nor topographic ridge directions (Mudry and Rosenthal 1977; Chauve et al. 1986a, b; Perrin and Luetscher 2008).

Knickpoints 6–9 (Fig. 6) are localized along NE–SW directed thrusts, but also at the location of anthropogenic dams and have thus been discarded. Knickpoint 6 corresponds to the "Saut du Doubs" and the Chatelot dam. The "Saut du Doubs" is a natural waterfall resulting from the shift of the Doubs River after a large landslide event dated at ~12 ka (Campy et al. 1994; Bichet et al. 1999). The Chatelot dam, which was built downstream of this natural waterfall, creates a 3.3-km long lake and a 74 m high waterfall involving a high $k_{sn}$ value along the river profile (graph on Fig. 6, $k_{sn} = 1242$).

Neotectonic knickpoints highlighted along the upstream part of the Doubs River are localized along NE–SW directed thrusts and/or folds. Knickpoint 3 is localized at the junction between the N–S Pontarlier sinistral fault and the NE–SW fold axis. However, the left lateral strike-slip fault of Pontarlier cuts the fold axis at this location (Laubscher 1992; Homberg et al. 2004), and our field observations are in agreement with a purely horizontal displacement. Although displacements caused by pure strike slip faults theoretically cannot trigger disturbances along river longitudinal profiles, these fault zones can act as preferential drainage patterns potentially creating deep canyons (e.g., the narrow deep valley of the Doubs River, south of Pontarlier, Fig. 1). Landslides and rockslides may also occur along these canyons, subsequently triggering knickpoints (Phillips et al. 2010, Fig. 7). Consequently, the knickpoint 3 can either be interpreted as resulting from an anticline growing or from landsliding/rocksliding triggered by fault activity. Thus, it has not been interpreted as a neotectonic signal.

In its easternmost part, the Doubs is sharply turning toward the west (near Saint-Ursanne, Fig. 6). This zone corresponds to a highly deformed area where several neotectonically controlled knickpoints occur (knickpoints 12–16 on Fig. 6). These knickpoints are the most-striking neotectonic signals observed along the Doubs. Here, the High and External Ranges are geographically joining and topographic structures resulting from this junction may be one reason for the half turn evidenced by the river. Between Saint-Ursanne and Montbéliard (Fig. 6) the Doubs River has a dual behavior: (i) it flows following major tectonic structures toward the west in the upstream part (subsequent river); and (ii) it turns toward the northwest at Dessoubre junction, crossing structures (antecedent river). Knickpoint 19 (Fig. 6) corresponds to the intersection between an E–W directed thrust and fold and a N–S normal fault. Both could control this knickpoint and our analysis cannot allow us to distinguish the dominant structure.

Along its third part (downstream of Montbéliard, Fig. 6), the Doubs flows through an area affected by N–S

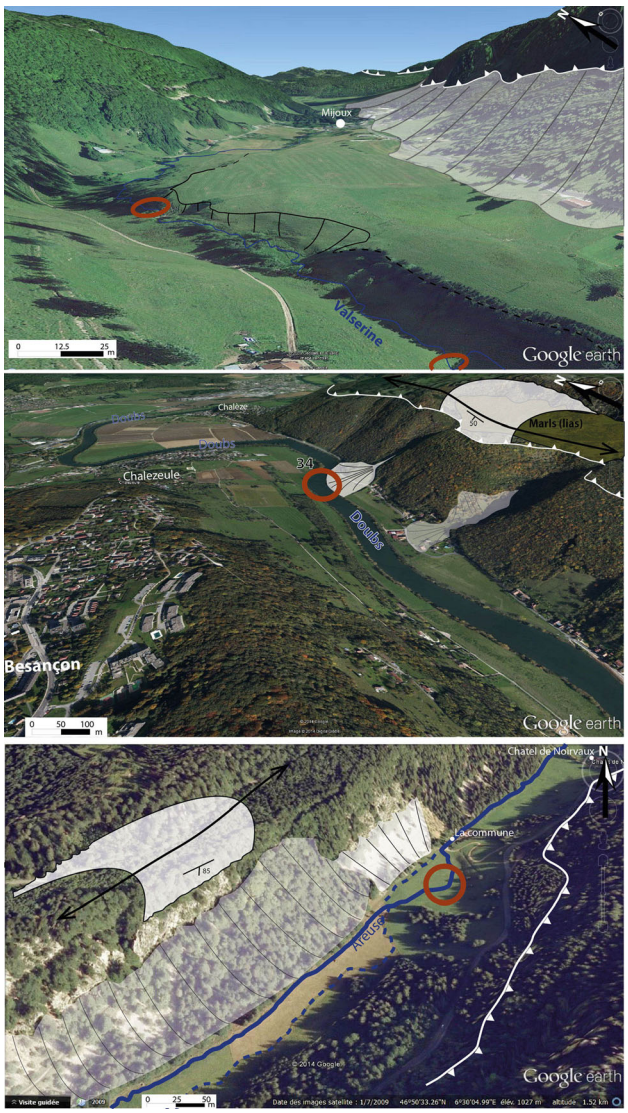


**Fig. 7** Field observations along flow paths of the Valserine, Doubs and Areuse rivers (see Fig. 4 for locations). **a** Valserine valley path in the High Range of the Jura Mountains. The NE–SW directed thrust created a topographic relief, which results in several landslides and rockslides. This valley was filled by glacial deposits and the river incision created a step involving frequent landslides which are correlated with knickpoint location (*red circles*). **b** The Doubs River upstream Besançon (External Range). The ENE-WSW directed thrust combined with erosion of the anticline hinge created landslides and rockslides. The younger one (in *white*) is correlated with knickpoint location (*red circle*, knickpoint 34 on Fig. 6). **c** The Areuse steep sided valley trough the High Range. This valley corresponds to a remnant syncline between two NE–SW directed tight folds. The southeastern most one is over-thrusted on the syncline decreasing the valley width. The anticline on *left side* of the river has a very steep southwestern flank involving frequent landslides and rockslides. On this picture at least two rockslides can be determined; an old one (in *transparent light grey*) already covered by a forest and a younger one (in *transparent white*) not yet covered by vegetation. It is still possible to see the ancient river path (in *blue dot line*). The river has presently restored its path following the older landsliding disturbance but remains deviated by the more recent one, which corresponds to a knickpoint location (*red circle*)

normal faults corresponding to the RBTZ (Lacombe et al. 1990; Becker 2000; Madritsch 2008) before flowing across the External Range (Besançon Range BR, Fig. 6). Among the 20 knickpoints identified, 9 can be interpreted as resulting from neotectonic forcing (knickpoints 23, 27, 29, 30, 32, 36, 37, 38 and 40 on Fig. 6). Along the RBTZ, the Doubs River crosses several normal faults, unfortunately many anthropogenic dams have been built in this section. Although most of these dams correspond to thresholds dams (lower than 5 m high), which are generally built on pre-existing topographic thresholds, we prefer not to interpret these knickpoints as evidence for any potential tectonic forcing and have thus discarded them. Across the Besançon Range (External Range), knickpoints occur along NE–SW thrusts and folds but only some of them could be interpreted as neotectonic signals.

In summary, the longitudinal profile of Doubs River is highly affected by structural patterns of the Jura Mountains. Neotectonic knickpoints occur both in the High and External Ranges, and the most-striking signals occur where the two ranges merge at the northern tip if the Jura arc.

### 4.2 The Ain River: a river highly influenced by anthropogenic factors

The Ain River drains the intermediate plateau of the Jura and flows mainly on glacial alluvial cover and limestone bedrock (Fig. 8). It is fed by both karst springs and surface runoffs and flows over ~190 km before joining the Rhône River at the southern end of the Jura. The karst spring, known as the "Source de l'Ain" (upstream of the yellow star "a" in Fig. 8), corresponds to a Vauclusian spring (spring fed by overflow), which can be disconnected from the river during low water periods. Indeed, the groundwater network feeding this river consists of two superposed levels with the main surface outlet located farther downstream of the "Source de l'Ain" (yellow star "a" in Fig. 8), while the "Source de l'Ain" spring corresponds to the upper-level overflow. The Ain is also fed by three surface runoffs (Serpentine, Saine and Lemine Rivers, Fig. 8), and flows westward before shifting southward where it is constrained by the Heute and Lons Ranges (Fig. 8).

The Ain can be divided into three different segments: (i) the upstream part (knickpoints 1, 2 and 3 on Fig. 8) corresponding to a tectonically-deformed area with high temporal and spatial discharge variations, (ii) the middle section (from knickpoint 4–15 on Fig. 8) flowing through the undeformed intermediate plateau, and (iii) the downstream section flowing westward and crossing the folded and overlapped structures of the Lons Range (LR, Figs. 1, 8).

Many artificial dams have been built along the Ain, inducing the most-striking signals along its longitudinal profile (Fig. 8). The Vouglans dam is the biggest dam built along the river (103-m high, 427-m long with a 1120 $km^2$ impounded drainage area) and involves very high $k_{sn}$ values (knickpoint 15 on Fig. 8, $k_{sn} = 3622$). These anthropogenic factors overprint any potential neotectonically controlled knickpoints. The influence of the Vouglans dam on the river profile cannot be precisely quantified, but given that its impounded drainage area does not exceed the 35 % of the total drainage area of the Ain River (3765 $km^2$) and that the river width immediately downstream of the dam is around 50 m, we can estimate that its impact on the river profile is only limited over less than ~1 km downstream (e.g., Brandt 2000).

The hydrological regime along the first river segment (knickpoints 1–3 on Fig. 8) is complex due to high discharge variations of both the Vauclusian karst spring and the permanent surface runoffs, especially along the Saine and the Lemine rivers (south of knickpoint 3, Fig. 8). Knickpoints 2 and 3 mainly result from the complex karst system ("Source de l'Ain" and "Sources de la Papeterie", Fig. 8). Knickpoint 3 ("Perte de l'Ain", Fig. 8) corresponds to a local karst complex where most of the river discharge goes through seepage underground along 100 m before returning to the river farther downstream. It also corresponds to a structural junction between N20°E and N50°E oriented tight folds and thrusts and a N–S trending left-lateral strike-slip fault. However, the strong karst signals overprint any potential neotectonic signal and prevent us from any tectonic interpretation in this area.

In its middle part (from knickpoint 4–15 on Fig. 8), the Ain flows on a barely deformed plateau. At this location, this river seems to be blocked on its right bank by the "Heute Faisceaux" and flows southward following the dip-direction of the plateau. Here, the Ain flows almost exclusively on glacial alluvium and reaches limestone bedrock only in a few places, involving lithologically-controlled knickpoints (knickpoints 6, 7, 8, 11, 12 and 13 on Fig. 8). Several dams and anthropogenic structures have also been built along this river section, resulting in low to moderate $k_{sn}$ values.

The downstream Ain section starts with knickpoint 16 (Fig. 8), corresponding to the Coiselet dam (25.5-m high). Here, the Ain River enters the Lons Range where the plateau is getting narrower and is affected by N20°E–N40°E oriented folds and thrusts. The Ain crosses different structures via transversal valleys, and neotectonically controlled knickpoints occur at these intersections (knickpoints 17, 20 and 22 on Fig. 8). These signals are located on N150°E–N180°E trending deformed zones, thrusts and/or fold axes which could involve neotectonic knickpoints.

In summary, the Ain River flows through two deformed areas separated by an undeformed plateau. In the first section, complex karst interactions induce morphological

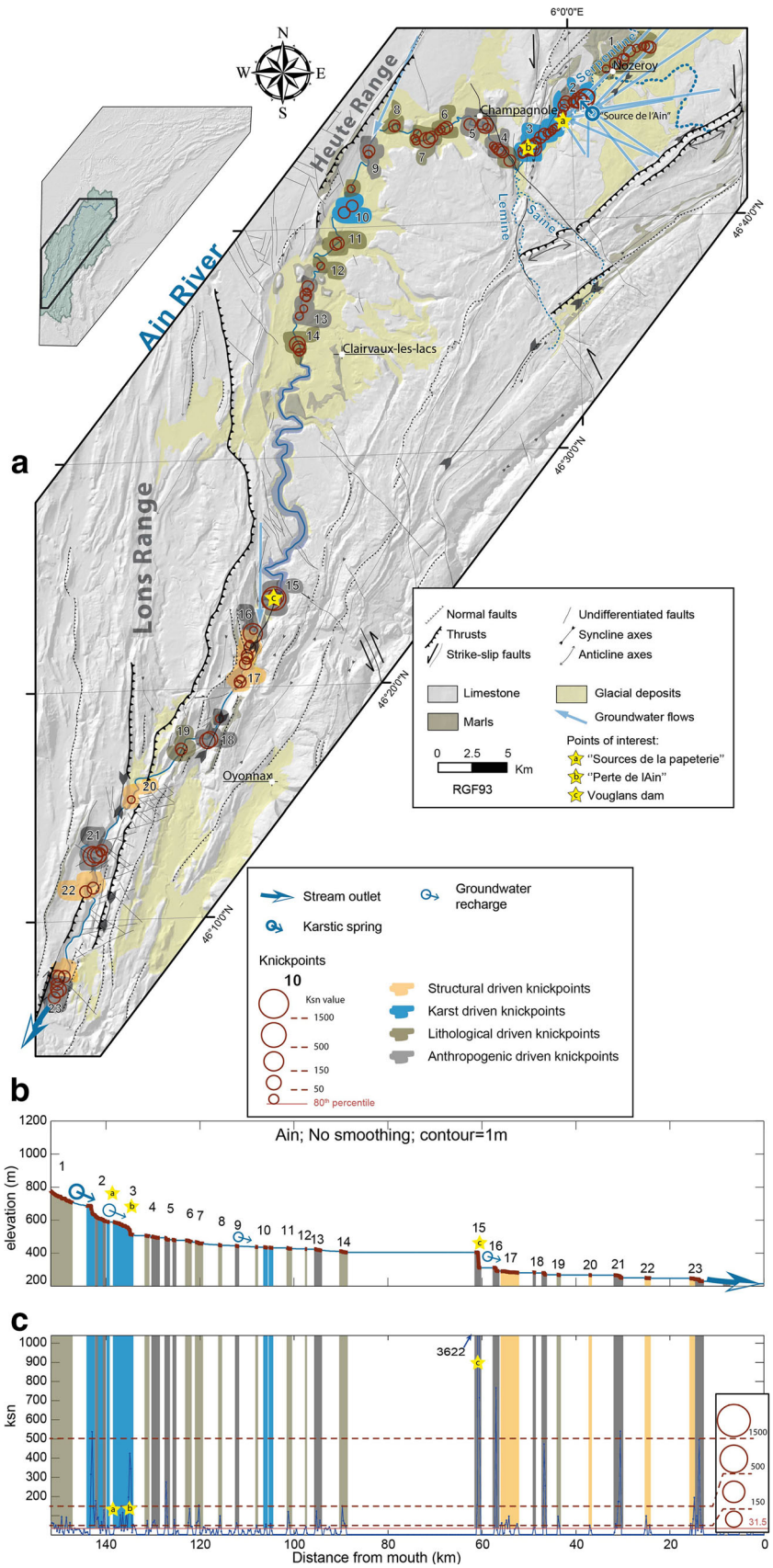


**Fig. 8** Map of the Ain River (**a**) and its longitudinal profile (**b**) and $k_{sn}$ evolution (**c**). Lithological, karst and structural details have been reported along the Ain. Knickpoints (*red circles*) have been located and classified in size by their intensities ($k_{sn}$ values). Each knickzone has been interpreted regarding geological, topographic and hydrological maps in term of potential lithological, structural, anthropogenic and karst forcing (for color code, see legend). See Sect. 4.2 for further details

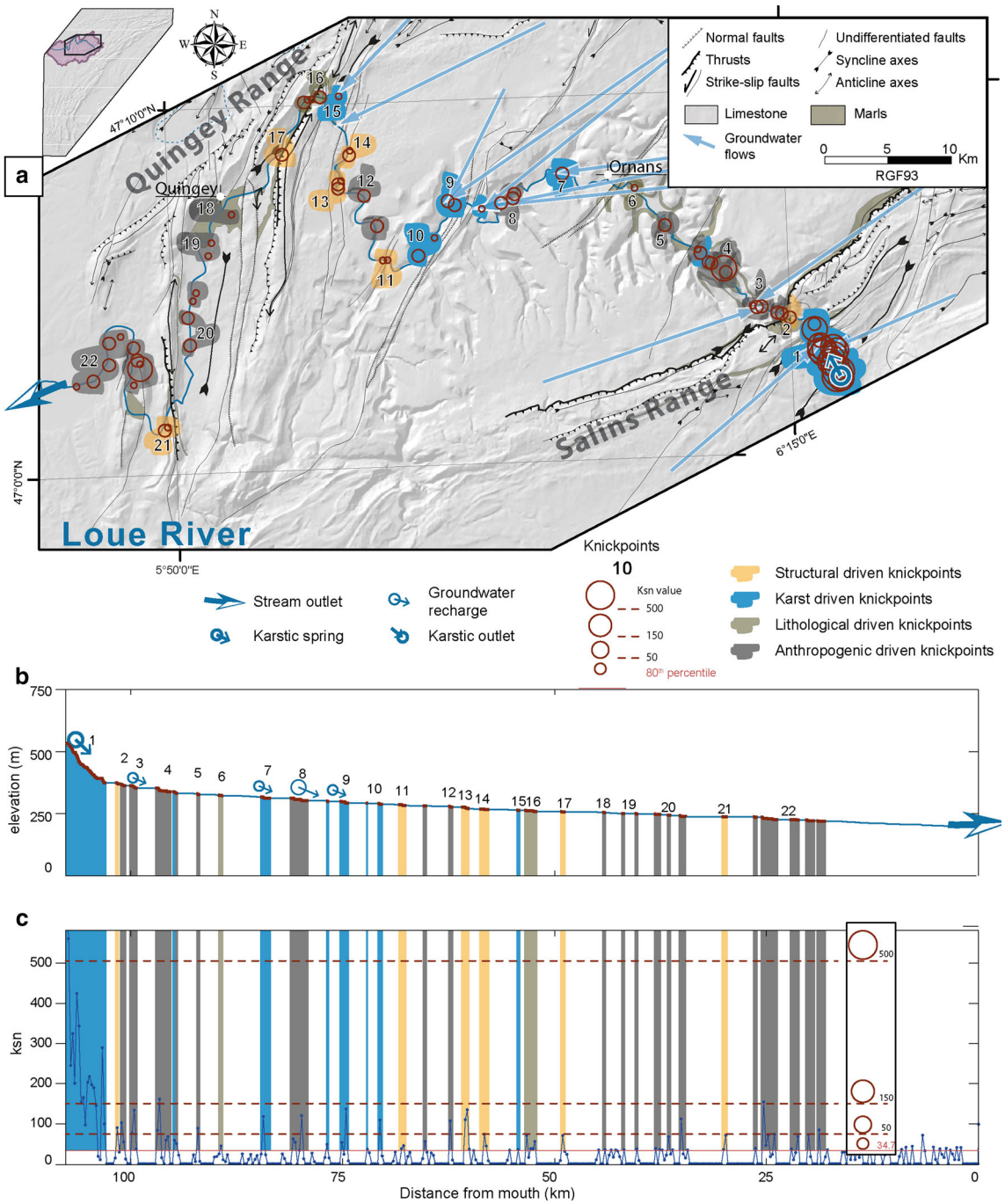


**Fig. 9** Map of the Loue River (**a**), its longitudinal profile (**b**) and $k_{sn}$ evolution (**c**). Lithological, karst and structural details have been reported on the along the Loue path. Knickpoints (*red circles*) have been located and classified in size by their intensities ($k_{sn}$ values). Each knickzone has been interpreted regarding geological, topographic and hydrological maps in term of potential lithological, structural, anthropogenic and karst forcing (color code, see legend on the figure). The Loue River is a karst river mainly fed by the Doubs River (Fig. 6). See Sect. 4.3 for further details

signals that overprint potential neotectonic knickpoints. On the contrary, the intermediate plateau is dominated by anthropogenic and lithological influences. In the Lons Range, our profile analysis highlights potential neotectonic activity along thrusts and folds.

### 4.3 The Loue River: a karst network

The Loue River is fed by a karst spring (Fig. 9) and flows over 130 km along the Ornans plateau after crossing the Salins Range (Figs. 1, 9). This river corresponds to an

open-pit karst collector, which is largely fed by karst tributaries along its first part (Fig. 9) and partly fed by the Doubs River through seepages near Pontarlier (e.g., Mudry and Rosenthal 1977, Fig. 6).

The Loue can be divided into three segments (Fig. 9): (i) the upstream part, flowing through the Salins Range and corresponding to narrow gorges crossing several folds; (ii) the middle part between the Salins and Quingey Ranges, corresponding to a karst plateau where the river flows broadly toward the west; (iii) the third downstream segment, which flows across the Quingey Range. Here, the river follows syncline axes and exits the Jura to the west where the Quingey and Salins Ranges join together.

The first segment exhibits many knickpoints associated with very high $k_{sn}$ values (from 200 to more than 500). The Loue spring is a highly complex karst system (Chauve et al. 1986a, b) which results in an important knickzone at the surface (knickpoint 1 on Fig. 9). Even though the river crosses tectonic structures in this area, the karst overprint inhibits any discrimination of neotectonically controlled disturbance signals. Only knickpoint 2 can be interpreted as resulting from the structural pattern, as no major karst spring occurs at this location where the river crosses a major frontal thrust of the Salins Range (Fig. 9).

The second river segment corresponds to the plateau area. Knickpoint signals along its southwestern part mainly evidence anthropogenic thresholds dams (knickpoints 3–6 on Fig. 9), whereas knickpoints 7–10 are mainly of karst origin. Each karst spring along the Loue River involves a moderate knickpoint ($50 < k_{sn} < 150$), while knickpoint 10 ($k_{sn} \sim 100$) potentially corresponds to diffuse karst springs associated to NE–SW normal faults. Knickpoints 11, 13 and 14 (Fig. 9) are located along NE–SW faults and could highlight a neotectonic control, with moderate to high $k_{sn}$ values ($\sim 150$ for knickpoint 13).

Along its third segment the Loue flows through the Quingey Range. Unfortunately, several anthropogenic dams occur along this downstream part (knickpoints 18–22 on Fig. 9) but some neotectonic signals can still be discriminated. Knickpoints 16, 17 and 21 correspond to major N–S to NE–SW thrusts, where transversal valleys are quite large without steep sides. Even though some rockslide deposits have been identified near the knickpoint 16 during our field investigations, this is not the case for knickpoints 17 and 21. This suggests that they can be considered as markers of neotectonic activity.

In summary, the main information from the Loue is that high $k_{sn}$ values along the first section seem to be controlled by both groundwater resurgences and anthropogenic features, probably overprinting neotectonically controlled evidence along the Loue River.

**Fig. 10** **a** General map of knickpoints in the Jura Mountains. The neotectonically controlled knickpoints determined along sixteen river profiles are shown in the simplified structural map (*orange circles*). Knickpoints have been classified in size by their intensities ($k_{sn}$ values). River profiles point towards neotectonic activity in both the High Range and the External Range. The *white map* inserted in the *high left corner* highlights the gradient of $k_{sn}$ intensity between the High Range (high values) and the External Range (low values). The *white map* inserted at the *right side of the general map* represents the LGM ice extent along with the distribution of $k_{sn}$ intensities. The diameter of the circles refers to the four categories of $k_{sn}$ intensities defined in legend. **b** The frequencies diagram of $k_{sn}$ intensities shows a large proportion of moderate signals ($50 < k_{sn} < 150$), which occurs all over the Jura Mountains. **c** $K_{sn}$ values versus the drainage area shows no direct relation between these two variables. (see Sects. 4.4 and 5.2 for further details)

### 4.4 General map

In this section, we compile the overall database of neotectonically controlled knickpoints used as a proxy for neotectonic activity and classified by $k_{sn}$ magnitudes in order to draw a general $k_{sn}$ map over the Jura Mountains (Fig. 10). A total of 5808 knickpoints have been identified in the overall Jura Mountains, however after our very careful checking, only 409 of them (7 % of the total) could be unambiguously interpreted as having a neotectonic control. $k_{sn}$ intensities reach up to 1240 but 97 % of the values are lower than 500 (Fig. 10b), confirming the low disturbances triggered by neotectonics compared to other potential factors.

Concerning the tectonic-related signals, the frequency diagram and map of $k_{sn}$ intensities (Fig. 10a, b) show that about 80 % of the observed signals correspond to $k_{sn}$ value $<150$ and are distributed in the overall Jura Mountains. However, more than 50 % of $k_{sn} < 150$ are located along the External Range. About 68 % of knickpoints, ranging between 150 and 500 in intensities, are distributed along the High Range and the northern part of the External Range. Finally most prominent river disturbances ($k_{sn} > 500$) are all located along the High Range (Fig. 10a).

The distribution of knickpoint intensities along the rivers shows that $k_{sn}$ magnitudes are not directly correlated neither with the local slope, the elevation, nor the drainage area (Fig. 6c, supplementary material). Indeed, looking at some key examples such as the Valserine River (river 15 in Fig. 10), the Orbe River (river 8 in Fig. 10) and the Dessoubre River (river 4 in Fig. 10) confirms the absence of correlation with morphometric indicators. Indeed, the Valserine highlights higher $k_{sn}$ in its downstream part (lower slopes and elevations, higher drainage area) than in its upstream part (higher slopes and elevations, lower drainage area) whereas the Dessoubre highlights the exact opposite distribution. Moreover, the Orbe shows high

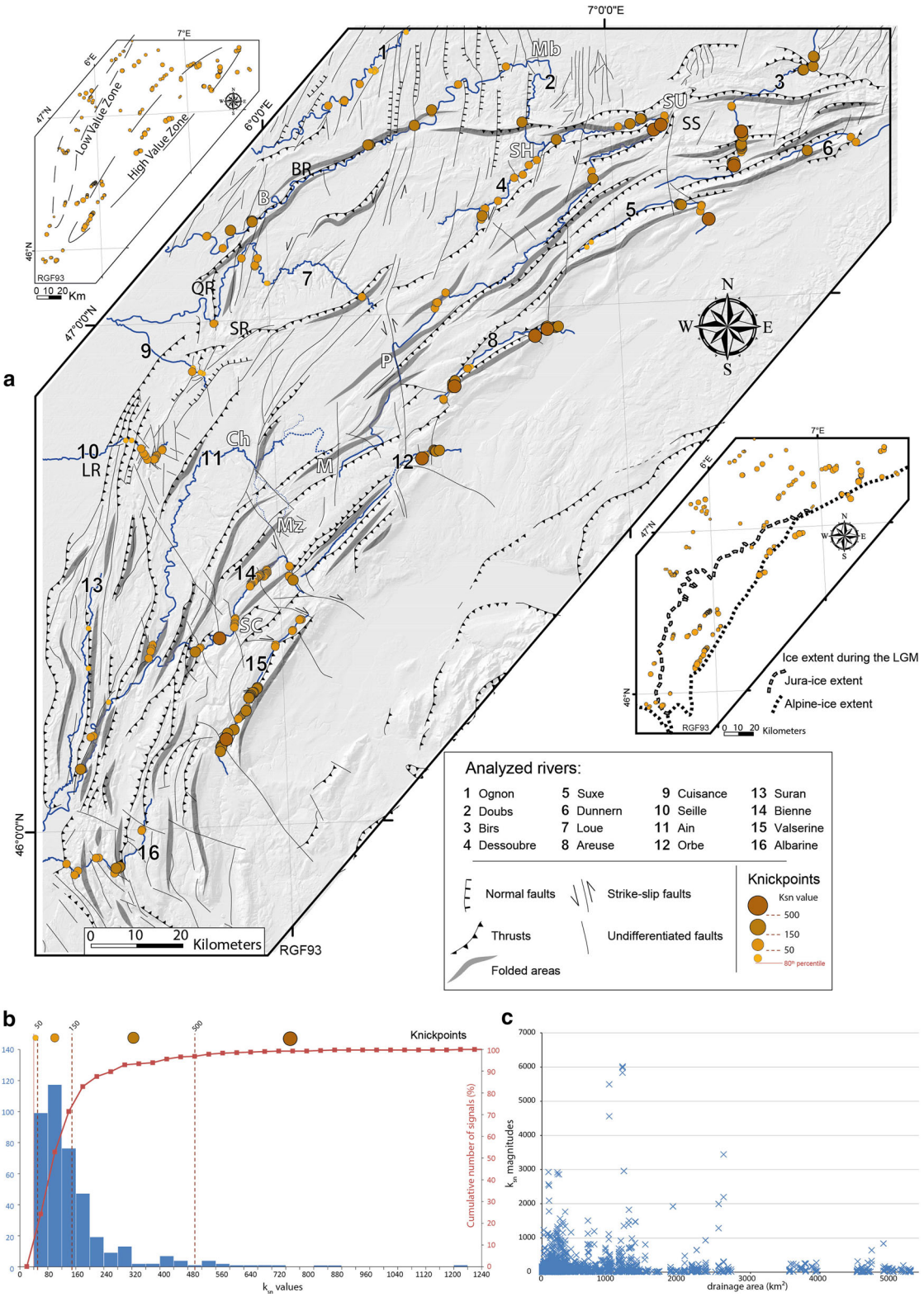
a
7°0'0"E
6°0'0"E
47°0'0"N
46°0'0"N
Mb
SU
SS
SH
BR
B
OR
SR
P
Ch
M
Mz
SC
LR
1
2
3
4
5
6
7
8
9
10
11
12
13
14
15
16
N
S
W
E
0 10 20 Km
RGF93
Low Value Zone
High Value Zone
Ice extent during the LGM
Jura-ice extent
Alpine-ice extent
0 10 20 Kilometers
Analyzed rivers:
1 Ognon
2 Doubs
3 Birs
4 Dessoubre
5 Suxe
6 Dunnern
7 Loue
8 Areuse
9 Cuisance
10 Seille
11 Ain
12 Orbe
13 Suran
14 Bienne
15 Valserine
16 Albarine
Normal faults
Strike-slip faults
Thrusts
Undifferentiated faults
Folded areas
Knickpoints
Ksn value
500
150
50
80th percentile
b
Knickpoints
Number of signals
Cumulative number of signals (%)
k_sn values
c
k_sn magnitudes
drainage area (km²)

knickpoints in both its downstream and in its upstream part (Fig. 10a, c; Appendix 5 in the supplementary material). Finally, the insert map in Fig. 6 shows that there is no spatial correlation between the distribution of $k_{sn}$ intensities and the LGM ice extent.

This spatial distribution of knickpoint intensities potentially highlights a higher tectonic activity in the High Range compared to the External Range. Knickpoints are mainly located along thrusts and folds, but transversal faults could also generate low to moderate signals whereas rare knickpoints are associated to normal faults (Fig. 10).

In the western part (Lons Range, LR on Fig. 10), only few knickpoints are located along tectonic structures (normal faults and thrusts, rivers 9, 10 and 13 on Fig. 10). This region is under the Bresse Graben influence (Becker 2000), characterized by normal faults which involve knickpoints at the western side of the plateau. This plateau is also affected by a particular erosion pattern called "reculées" (regressive erosion), which could involve knickpoints. These "reculées" correspond to steeply incised valleys which result from preferential erosion of cold and aggressive water (i.e., with high $CO_2$ concentrations) along faults (Bailly et al. 1975 and references therein). Part of the signals detected in this area corresponds to such "reculées".

The northernmost part of the Jura Mountains (Montbéliard area, Mb on Fig. 10) is also affected by N-S directed normal faults due to the RBTZ (Lacombe et al. 1990; Becker 2000; Madritsch et al. 2009). The lack of knickpoints along the Doubs profile (river 2 on Fig. 10) when flowing in the vicinity of these normal faults is not decisive for recent quiescence along these tectonic structures; indeed the presence of many man-made dams along this river section may inhibit the identification of any clear neotectonic signal (see Sect. 4.1). Moreover, the Ognon profile (river 1 on Fig. 10) presents some neotectonically controlled knickpoints along the same N–S faults, which suggests a potential neotectonic activity along these structures, as already suggested by Madritsch et al. (2012).

## 5 Discussion

### 5.1 Formation and evolution of river knickpoints

#### *5.1.1 Knickpoint triggering factors*

Recent studies have shown that many different factors, including weathering, differential erosion rates, as well as headwater capture can drive disequilibrium in river stream profiles (Yanites et al. 2013; Willett et al. 2014), thereby inducing knickpoint development. These factors may supplement those already known, such as lithological contrasts, anthropogenic disturbances and long-term tectonic or climatic forcing (e.g., Phillips et al. 2010; Walsh et al., 2012). In turn, it is difficult to decipher their relative role from morphometric analysis.

Our study shows that groundwater flow in karst domains also represents an important disturbing factor when estimating the contributing drainage area that is commonly used as a proxy for river discharge. The underground network complexity, encompassing crossings between surface runoffs and other underground networks, karst captures and diffuse outlets, results in many potential disturbances along the river profiles as well as biases in calculating the contributing discharge area. All these complexities may induce deviations from a theoretical river profile based on the stream power model. In this context it is important to use a normalized $k_s$ parameter (see Sect. 3.2) and to confront knickpoint locations a posteriori with available hydrological maps and information. This comparison has been possible in the Jura case, thanks to our good knowledge of the karst systems (Mudry and Rosenthal 1977; Chauve et al. 1986a, b; Bichet et al. 1999; Charlier et al., 2012; Calmels et al. 2014).

Our study also shows that, in the case of the Jura, all the above-mentioned different factors can overprint each other and can be classified with respect to their induced-knickpoint intensity: (i) anthropogenic disturbances (high magnitude); (ii) karst imprint (medium magnitude); and (iii) lithological contrast, landslides and neotectonic controls (lower magnitude). All the three factors could spatially coexist and would induce geomorphological signals of similar amplitude.

#### *5.1.2 Transient nature of knickpoints*

Whipple and Tucker (1999) have shown that a disturbed river, either by a sudden base level fall or a localized increase in the uplift rate, will restore its equilibrium by an upstream migration of the newly created knickpoint. This migrating wave could potentially erase all evidence of previous disturbances along longitudinal profiles. Thereby the typical response time (i.e., the wave speed) will depend on rock strength, magnitude of the disturbance and climatic factors.

In the Jura Mountains, many of the potential parameters influencing this characteristic response time are still unknown. Although rock strength is relatively homogeneous (limestones), the rock uplift rate and its spatial variations remain important unknowns. Climatic changes during Quaternary times seem to have had only a minor influence on the longitudinal profiles in a slowly uplifting context and could thus to some extent be discarded in the Jura case (Carretier et al. 2006). Another poorly known parameter that will strongly influence the response time of

the river to perturbations is the incision rate in limestone bedrock. Limestone is very sensitive to erosion, and incision rates over this bedrock lithology depend on both CO2 concentrations and the nature of transported sediments. Monbaron (1975) proposed an incision rate of 0.42 mm/year in the Sorne River (see the Sorne Syncline (SS) on Fig. 1), while Aubert (1969 and references therein) quantified chemical erosion rates of 0.1 mm/year over the whole Jura Mountains. However, no evidence of spatially-uniform incision rate over the whole Jura could be expected, as fluvial incision rates can be disturbed by sediment traps or underground water flows which induce variations in water discharges and thus in river transport and incision capacity.

All these unknown parameters prevent us from a correct estimation of the river response time to perturbations in the case of the Jura Mountains. However, rivers are expected to potentially preserve topographic anomalies caused by uplift rate variations over about tens of thousands years (e.g., Whipple and Tucker 1999; Carretier et al. 2006). Considering the total reset of most of the Jura rivers during the last ice extent, and according to previous studies (Nivière and Winter 2000; Carretier et al. 2006; Madritsch et al. 2010a; Molliex et al. 2011), our analyzed river profiles are expected to have preserved the most recent tectonic disturbances.

## 5.2 Current deformation style of the Jura Mountains

### *5.2.1 General spatial distribution of neotectonic signals*

After a careful identification and selection of the unambiguous neotectonically controlled knickpoints, we have established a spatial correlation between river knickpoints and the main tectonic structures (see Sect. 4.4, Fig. 10). The internal High Range shows higher $k_{sn}$ values on average than the External Range, with a decreasing gradient in $k_{sn}$ magnitudes toward the north-west (Fig. 10). This spatial distribution cannot be explained by a gradient in precipitation; these are quite homogeneous over the Jura (Frei and Schar 1998; Calmels et al. 2014). Indeed, we propose that this $k_{sn}$ distribution reflects differential neotectonic activity across the Jura arc. Our observations are qualitatively in agreement with modern uplift estimates of 0.1–1.1 mm/year using leveling (Jouanne et al. 1995, 1998) in the southern part of the High Range, and with long-term uplift estimates between 0.05 and 0.17 mm/year from morphological analyses in the External Range (Giamboni et al. 2004b; Ustaszewski and Schmid 2007; Madritsch et al. 2010b; Molliex et al. 2011).

### *5.2.2 Hypothesis regarding ongoing shortening*

The tectonic activity highlighted in the External Range could be related to the growth of anticlines and associated horizontal shortening in the frontal part of the Jura Mountains during Plio-Pleistocene times (considering no glacial-reset in the Northern Jura, see Sect. 2.3), as already proposed by several authors (Ustaszewski and Schmid 2007; Madritsch et al. 2010a, b; Molliex et al. 2011). Analog and numerical models suggest that the deformation style of accretionary wedges and fold-and-thrust belts strongly depends on the coefficient of elemental-wall friction (friction between displaced materials and basement, Burbidge and Braun 2002; Smit 2005). In study cases similar to the Jura Mountains, where the elemental-wall friction is accommodated by an evaporitic basal décollement (very low friction coefficient), the dominant deformation mode is frontal accretion associated with "pop-up" structures, and the deformation is only marginally accommodated by retro thrusts in the High Range. Indeed, temporal and/or lateral spatial variations of heterogeneous element-wall friction coefficients (see for instance Burbidge and Braun 2002), could have occurred, inducing oscillations between frontal thrusting and back-thrusting. Moreover, the deformation style of the Jura is expected to have changed during Pliocene times from a thin-skinned to a thick-skinned mode (Mosar 1999; Becker 2000; Lacombe and Mouthereau 2002; Ustaszewski and Schmid 2007). This change would imply that the Triassic evaporites no longer played their role of a decoupling level and most of the uplift would, in this case (strong friction coefficient), be expected to be concentrated near the back of the wedge, in combination with underthrusting (Burbidge and Braun 2002). The hypothesis of (re)activation of backthrusts in the internal part of the Jura arc would fit our observations showing higher neotectonic movements in the High Range (internal chain) compared to the External Range (frontal chain).

### *5.2.3 Isostatically driven uplift in the Jura arc*

Since the 90's, isostatic mechanisms have been invoked to explain that part of the observed rock uplift that cannot be entirely explained by crustal thickening (England and Molnar 1990 and references therein; Hatfield et al. 1991). Here we propose an alternative geodynamic model, considering the orogenic system Alps-Jura to explain both the relatively high uplift rates observed in the High Range and their northwestward decrease. The Plio-Pleistocene to present-day rock uplift (Serpelloni et al. 2013) and exhumation (Fox et al. 2015) documented in the European western and central Alps could be partly explained by an

erosion-driven isostatic rebound (Schlunegger and Hinderer 2003; Cederbom et al. 2004; Champagnac et al. 2007, 2009; van der Beek and Bourbon 2008; Valla et al. 2011) and/or by deep-seated processes such as slab breakoff (Sue et al. 1999; Lippitsch et al. 2003; Baran et al. 2014; Fox et al. 2015). In the Alpine realm, including the Jura arc, Serpelloni et al. (2013) established a positive correlation between uplift rates and topography, with uplift rates ranging from 1 to 3 mm/year in the core of the Alps, and from 0.5 to 1.5 mm/year within the Jura Mountains. This correlation potentially reveals a causal link between the measured uplift and buoyancy forces within the alpine root and/or erosional surface processes. Using numerical modeling coupled with morphometry, Champagnac et al. (2007) have proposed that the isostatic rebound induced by Quaternary erosion could imply uplift rates both in the Alps ($\sim$0.5 mm/year) and in the Jura (up to 0.2 mm/year in the High Range). An alternative, but not exclusive, hypothesis would imply slab detachment (Lippitsch et al. 2003; Baran et al. 2014; Fox et al. 2015) as a driving mechanism for recent uplift in the Alpine realm. In this framework, the spatial gradient we observed from the High Range towards the External Range would also fit with this hypothesis, implying mainly intrinsic buoyancy forces as a key factor in the current Alps-Jura dynamics.

Unloading induced by deglaciation has also been discussed as a driver of isostatic rebound (Gudmundsson 1994; Persaud and Pfiffner 2004; Barletta et al. 2006; Sue et al. 2007; Stocchi and Spada 2009; Norton and Hampel 2010). Norton and Hampel (2010) have shown that the isostatic adjustment rates in the Alps could range between 14 and 25 mm/year during the glacial overload and glacial retreat times, respectively. These authors suggest that the isostatic rebound is almost fully achieved in the 6 ka following the ice retreat and only residual rates persist since 15 ka. Moreover, as shown on the Fig. 10, our analysis does not show any correlation between the high density of knickpoints and the LGM ice extent.

## 6 Conclusions

Morphological signals along the Jura river profiles are the result of one or several of the four controlling factors, which are, in decreasing order of disturbance magnitudes: (i) anthropogenic imprint; (ii) groundwater flow impacting river discharge and erosional capacity; (iii) tectonic forcing; and (iv) lithological control. River profile analysis in karst domains requires the use of a steepness parameter normalized by the drainage area, in combination with a careful cross-check of the location of each knickpoint with respect to the groundwater network.

In the Jura Mountains, significant neotectonic activity has been characterized by longitudinal river profile analyses, using knickpoints as first-order qualitative proxies. Although this activity seems to have been recorded over the entire Jura arc, it appears to be higher in the High Range than in the External Range (Fig. 10). This particular spatial distribution could be related to an ongoing horizontal shortening in the External Range, and/or to isostatic processes linked to the Alps-Jura orogenic system (erosional unloading and/or deep-seated processes) acting over Quaternary times. These results are in agreement with previous geodetic data and geomorphological observations indicating highest uplift rates in the High Range, associated with horizontal shortening which persists at least until Pleistocene times at the Jura front. Nonetheless, our results do not allow us to further discriminate between an ongoing shortening or isostatic mechanisms.

Although the neotectonic deformation along the Jura Mountains remains (very) moderate, our study reveals that focusing on geomorphic evidence allows deciphering recent tectonic activity along the arc, and more specifically in the High Range. This approach could be further developed to better, and quantitatively, constrain the late stages of deformation in the Jura and the potential triggering mechanisms.

**Acknowledgments** We thank the editor S. Schmid, H. Madritsch and three anonymous reviewers for their constructive comments that helped to improve our manuscript. This study was funded by the French Research Minister and the OSU THETA (Besançon observatory) to M.R. and C.S. P.G.V. acknowledges the funding from the Swiss National Foundation (Grant #PZ00P2_148191). The IGN is thanked for giving access to their topographic data. We are grateful to A. Vallet for his precious help on Matlab code and statistic treatments.

## References

Affolter, T., & Gratier, J. P. (2004). Map view retrodeformation of an arcuate fold-and-thrust belt: The Jura case. *Journal of Geophysical Research: Solid Earth,*. doi:10.1029/2002JB002270.

Aubert, D. (1949). Le Jura. *Geologische Rundschau, 37*, 2–17. doi:10.1007/BF01792491.

Aubert, D. (1969). *Phénomènes et formes du karst jurassien*. Basel: Birkhaüses.

Bailly, A., Chapus, R., Fontaine, J., Frachon, J. C., Nardy, J. P., Odouze, A. M., et al. (1975). *Éléments de géographie comtoise*. Besançon: Presses Univ. Franche-Comté.

Baran, R., Friedrich, A. M., & Schlunegger, F. (2014). The late Miocene to Holocene erosion pattern of the Alpine foreland basin reflects Eurasian slab unloading beneath the western Alps rather than global climate change. *Lithosphere, 6*, 124–131. doi:10.1130/L307.1.

Barletta, V. R., Ferrari, C., Diolaiuti, G., Carnielli, T., Sabadini, R., & Smiraglia, C. (2006). Glacier shrinkage and modeled uplift of the

Alps. *Geophysical Reseach Letters, 33*, L14307. doi:10.1029/2006GL026490.

Becker, A. (2000). The Jura Mountains—An active foreland fold-and-thrust belt? *Tectonophysics, 321*, 381–406. doi:10.1016/S0040-1951(00)00089-5.

Bichet, V., Campy, M., Buoncristiani, J.-F., Digiovanni, C., Meybeck, M., & Richard, H. (1999). Variations in sediment yield from the Upper Doubs River carbonate watershed (Jura, France) since the Late-Glacial Period. *Quaternary Research, 51*, 267–279. doi:10.1006/qres.1999.2037.

Brandt, S. A. (2000). Classification of geomorphological effects downstream of dams. *CATENA, 40*, 375–401. doi:10.1016/S0341-8162(00)00093-X.

Buoncristiani, J. F., & Campy M. (2001). Late Pleistocene detrital sediment yield of the Jura glacier, France. *Quaternary Research, 56*, 51–61. doi:10.1006/qres.2001.2243.

Buoncristiani, J. F., & Campy, M. (2004a). The palaeogeography of the last two glacial episodes in France: The Alps and Jura. In J. Ehlers & P. L. Gibbard (Eds.), *Developments in quaternary sciences, quaternary glaciations extent and chronology part I: Europe* (pp. 101–110). Amsterdam: Elsevier.

Buoncristiani, J. F., & Campy, M. (2004b). Expansion and retreat of the Jura ice sheet (France) during the last glacial maximum. *Sedimentary Geology, 165*, 253–264. doi:10.1016/j.sedgeo.2003.11.007.

Burbidge, D. R., & Braun, J. (2002). Numerical models of the evolution of accretionary wedges and fold-and-thrust belts using the distinct-element method. *Geophysical Journal International, 148*, 542–561. doi:10.1046/j.1365-246x.2002.01579.x.

Burkhard, M. (1990). Aspects of the large-scale Miocene deformation in the most external part of the Swiss Alps (sub-Alpine molasse to Jura fold belt). *Eclogae Geologicae Helvetiae, 83*, 559–583.

Burkhard, M., & Sommaruga, A. (1998). Evolution of the western Swiss Molasse basin: structural relations with the Alps and the jura belt. In A. Mascle, C. Puidefabregas, H. P. Luterbacher, & M. Fernandez (Eds.), *Cenozoic foreland basins of Western Europe* (pp. 279–298). London: Special Publication.

Calmels, D., Gaillardet, J., & François, L. (2014). Sensitivity of carbonate weathering to soil CO2 production by biological activity along a temperate climate transect. *Chemical Geology, 390*, 74–86. doi:10.1016/j.chemgeo.2014.10.010.

Campbell, I. (1964). Stream profiles and pediments. *Rocky Mountain Social Science Journal, 1*, 119–121.

Campy, M. (1982). *Le Quaternaire franc-comtois, essai chronologique et paléoclimatique*. Ph.D. thesis, Université de Franche-Comté, Besançon.

Campy, M. (1985). Dynamique d'une marge glaciaire au maximum würmien; La Combe d'Ain (Jura). *Bulletin de l'Association Française Pour L'étude du Quaternaire, 22*, 65–74. doi:10.3406/quate.1985.1530.

Campy, M. (1992). Palaeogeographical relationships between Alpine and Jura glaciers during the two last Pleistocene glaciations. *Palaeogeography, Palaeoclimatology, Palaeoecology, 93*, 1–12. doi:10.1016/0031-0182(92)90180-D.

Campy, M., Bichet, V., Giovanni, C. D., Richard, H., Richard, J., & Olive, P. (1994). Evolution des flux de matiere depuis 12 000 ans dans la haute vallee du Doubs (France). *Bulletin de la Societe Geologique de France, 165*, 381–400.

Carretier, S., Nivière, B., Giamboni, M., & Winter, T. (2006). Do river profiles record along-stream variations of low uplift rate? *Journal of Geophysical Research: Earth Surface, 111*, F02024. doi:10.1029/2005JF000419.

Castelltort, S., Goren, L., Willett, S. D., Champagnac, J.-D., Herman, F., & Braun, J. (2012). River drainage patterns in the New Zealand Alps primarily controlled by plate tectonic strain. *Nature Geoscience, 5*, 744–748. doi:10.1038/ngeo1582.

Cederbom, C. E., Sinclair, H. D., Schlunegger, F., & Rahn, M. K. (2004). Climate-induced rebound and exhumation of the European Alps. *Geology, 32*, 709–712. doi:10.1130/G20491.1.

Champagnac, J. D., Molnar, P., Anderson, R. S., Sue, C., & Delacou, B. (2007). Quaternary erosion-induced isostatic rebound in the western Alps. *Geology, 35*, 195–198. doi:10.1130/G23053A.1.

Champagnac, J.-D., Molnar, P., Sue, C., & Herman, F. (2012). Tectonics, climate, and mountain topography. *Journal of Geophysical Research: Solid Earth,*. doi:10.1029/2011JB008348.

Champagnac, J.-D., Schlunegger, F., Norton, K., von Blanckenburg, F., Abbühl, L. M., & Schwab, M. (2009). Erosion-driven uplift of the modern Central Alps. *Tectonophysics, 474*, 236–249. doi:10.1016/j.tecto.2009.02.024.

Charlier, J.-B., Bertrand, C., & Mudry, J. (2012). Conceptual hydrogeological model of flow and transport of dissolved organic carbon in a small Jura karst system. *Journal of Hydrology, 460–461*, 52–64. doi:10.1016/j.jhydrol.2012.06.043.

Chauve, P., Jacquemin, P., & Mania, J. (1986a). Representation des ecoulements en milieu karstique de zone plissee; exemple des hauts bassins du Doubs et de la Loue. *Bulletin de la Societe Geologique de France, 2*, 645–652.

Chauve, P., Mudry, J., Rosenthal, P., Tissot, G., & Tresse, P. (1986b). Role des abaissements d'axe dans les circulations karstiques du Jura. *Bulletin de la Societe Geologique de France, 2*, 329–336.

Coromina, G., & Fabbri, O. (2004). Late Palaeozoic NE–SW ductile–brittle extension in the La Serre horst, eastern France. *Comptes Rendus Geoscience, 336*, 75–84. doi:10.1016/j.crte.2003.09.019.

Coutterand, S. (2010). *Etude géomorphologique des flux glaciaires dans les Alpes nord-occidentales au Pléistocène récent: du maximum de la dernière glaciation aux premières étapes de la déglaciation*. Thesis, University of Chambéry.

Croissant, T., & Braun, J. (2014). Constraining the stream power law: a novel approach combining a landscape evolution model and an inversion method. *Earth Surface Dynamics Discussions, 2*, 155–166. doi:10.5194/esurf-2-155-2014.

Deichmann, N. (1992). Structural and rheological implications of lower-crustal earthquakes below northern Switzerland. *Physics of the Earth and Planetary Interiors, 69*, 270–280. doi:10.1016/0031-9201(92)90146-M.

Delacou, B., Sue, C., Nocquet, J.-M., Champagnac, J.-D., Allanic, C., & Burkhard, M. (2008). Quantification of strain rate in the Western Alps using geodesy: comparisons with seismotectonics. *Swiss Journal of Geosciences, 101*, 377–385. doi:10.1007/s00015-008-1271-3.

Demoulin, A. (1998). Testing the tectonic significance of some parameters of longitudinal river profiles: the case of the Ardenne (Belgium, NW Europe). *Geomorphology, 24*, 189–208. doi:10.1016/S0169-555X(98)00016-6.

Denizot, G. (1952). Le Pliocène dans la vallée du Rhône. *Revue de Géographie de Lyon, 27*, 327–357. doi:10.3406/geoca.1952.1144.

Dèzes, P., Schmid, S. M., & Ziegler, P. A. (2004). Evolution of the European Cenozoic Rift System: interaction of the Alpine and Pyrenean orogens with their foreland lithosphere. *Tectonophysics, 389*, 1–33. doi:10.1016/j.tecto.2004.06.011.

DiBiase, R. A., Whipple, K. X., Heimsath, A. M., & Ouimet, W. B. (2010). Landscape form and millennial erosion rates in the San Gabriel Mountains, CA. *Earth and Planetary Science Letters, 289*, 134–144. doi:10.1016/j.epsl.2009.10.036.

England, P., & Molnar, P. (1990). Surface uplift, uplift of rocks, and exhumation of rocks. *Geology, 18*, 1173–1177. doi:10.1130/0091-7613(1990)018<1173:SUUORA>2.3.CO;2.

Fournier, É. (1900). Les réseaux hydrographiques du Doubs et de la Loue dans leurs rapports avec la structure géologique. *Annales de Géographie, 9*, 219–228. doi:10.3406/geo.1900.6239.

Fox, M., Herman, F., Kissling, E., & Willett, S. D. (2015). Rapid exhumation in the Western Alps driven by slab detachment and glacial erosion. *Geology, G36411*, 1. doi:10.1130/G36411.1.

Frei, C., & Schar, C. (1998). A precipitation climatology of the Alps from high-resolution rain-gauge observations. *International Journal of Climatology, 18*, 873–900. doi:10.1002/(SICI)1097-0088(19980630)18:8<873:AID-JOC255>3.0.CO;2-9.

Giamboni, M., Ustaszewski, K., Schmid, S. M., Schumacher, M. E., & Wetzel, A. (2004a). Plio-Pleistocene transpressional reactivation of Paleozoic and Paleogene structures in the Rhine-Bresse transform zone (northern Switzerland and eastern France). *International Journal of Earth Sciences, 93*, 207–223. doi:10.1007/s00531-003-0375-2.

Giamboni, M., Wetzel, A., Nivière, B., & Schumacher, M. (2004b). Plio-Pleistocene folding in the southern Rhinegraben recorded by the evolution of the drainage network (Sundgau area; northwestern Switzerland and France). *Eclogae Geologicae Helvetiae, 97*, 17–31. doi:10.1007/s00015-004-1112-4.

Gibert, A. (1945). Remarques sur le réseau hydrographique du Jura. *Les Études Rhodaniennes, 20*, 246–252. doi:10.3406/geoca.1945.6611.

Goldrick, G., & Bishop, P. (2007). Regional analysis of bedrock stream long profiles: evaluation of Hack's. *Earth Surface Processes and Landforms, 32*, 649–671. doi:10.1002/esp.1413.

Golledge, N. R., Hubbard, A. L., & Sugden, D. E. (2009). Mass balance, flow and subglacial processes of a modelled Younger Dryas ice cap in Scotland. *Journal of Glaciology, 55*, 32–42. doi:10.3189/002214309788608967.

Golterman, H. L. (1982). La géochimie du Rhin et du Rhône et l'impact humain. *Hydrobiologia, 91–92*, 85–91. doi:10.1007/BF02391924.

Gudmundsson, G. (1994). An order-of-magnitude estimate of the current uplift-rates in Switzerland caused by the wurm alpine deglaciation. *Eclogae Geologicae Helvetiae, 87*, 545–557.

Hatfield, C. B., England, P., Molnar, P., Pinter, N., & Keller, E. A. (1991). Comments and replies on "Surface uplift, uplift of rocks, and exhumation of rocks". *Geology, 19*, 1051–1054. doi:10.1130/0091-7613(1991)019<1051:CAROSU>2.3.CO;2.

Heim, A. (1919). Geologie der Schweiz. Tauchnitz, Leipzig.

Henry, P., Deloule, E., & Michard, A. (1997). The erosion of the Alps: Nd isotopic and geochemical constraints on the sources of the peri-Alpine molasse sediments. *Earth and Planetary Science Letters, 146*, 627–644. doi:10.1016/S0012-821X(96)00252-X.

Hindle, D. (1997). *Quantifying strresses and strains from the Jura Arc, and their usefulness in choosing a deformation model for the region*. Thesis, University of Neuchatel.

Homberg, C., Angelier, J., Bergerat, F., & Lacombe, O. (2004). Using stress deflections to identify slip events in fault systems. *Earth and Planetary Science Letters, 217*, 409–424. doi:10.1016/S0012-821X(03)00586-7.

Homberg, C., Bergerat, F., Philippe, Y., Lacombe, O., & Angelier, J. (2002). Structural inheritance and cenozoic stress fields in the Jura fold-and-thrust belt (France). *Tectonophysics, Paleostresses and Tectonics in the Peri-Tethyan Margins, 357*, 137–158. doi:10.1016/S0040-1951(02)00366-9.

Homberg, C., Hu, J. C., Angelier, J., Bergerat, F., & Lacombe, O. (1997). Characterization of stress perturbations near major fault zones: Insights from 2-D distinct-element numerical modelling and field studies (Jura mountains). *Journal of Structural Geology, 19*, 703–718. doi:10.1016/S0191-8141(96)00104-6.

Homberg, C., Lacombe, O., Angelier, J., & Bergerat, F. (1999). New constraints for indentation mechanisms in arcuate belts from the Jura Mountains, France. *Geology, 27*, 827–830. doi:10.1130/0091-7613(1999)027<0827:NCFIMI>2.3.CO;2.

Howard, A. D. (1994). A detachment-limited model of drainage basin evolution. *Water Resources Research, 30*, 2261–2285. doi:10.1029/94WR00757.

Jackson, J., Norris, R., & Youngson, J. (1996). The structural evolution of active fault and fold systems in central Otago, New Zealand: Evidence revealed by drainage patterns. *Journal of Structural Geology, 18*, 217–234. doi:10.1016/S0191-8141(96)80046-0.

Jouanne, F., Genaudeau, N., Menard, G., & Darmendrail, X. (1998). Estimating present-day displacement fields and tectonic deformation in active mountain belts: an example from the Chartreuse Massif and the southern Jura Mountains, western Alps. *Tectonophysics, 296*, 403–419. doi:10.1016/S0040-1951(98)00156-5.

Jouanne, F., Menard, G., & Darmendrail, X. (1995). Present-day vertical displacements in the north-western Alps and southern Jura Mountains—Data from leveling comparisons. *Tectonics, 14*, 606–616. doi:10.1029/94TC03336.

Kastrup, U., Zoback, M. L., Deichmann, N., Evans, K. F., Giardini, D., & Michael, A. J. (2004). Stress field variations in the Swiss Alps and the northern Alpine foreland derived from inversion of fault plane solutions. *Journal of Geophysical Research: Solid Earth,*. doi:10.1029/2003JB002550.

Kirby, E., & Whipple, K. (2001). Quantifying differential rock-uplift rates via stream profile analysis. *Geology, 29*, 415–418. doi:10.1130/0091-7613(2001)029<0415:QDRURV>2.0.CO;2.

Kirby, E., & Whipple, K. X. (2012). Expression of active tectonics in erosional landscapes. *Journal of Structural Geology, 44*, 54–75. doi:10.1016/j.jsg.2012.07.009.

Kleman, J. (1994). Preservation of landforms under ice sheets and ice caps. *Geomorphology, 9*, 19–32. doi:10.1016/0169-555X(94)90028-0.

Kondolf, G. M. (1997). PROFILE: hungry water: effects of dams and gravel mining on river channels. *Environmental Management, 21*, 533–551. doi:10.1007/s002679900048.

Kühni, A., & Pfiffner, O. A. (2001). The relief of the Swiss Alps and adjacent areas and its relation to lithology and structure: topographic analysis from a 250-m DEM. *Geomorphology, 41*, 285–307. doi:10.1016/S0169-555X(01)00060-5.

Lacombe, O., Angelier, J., Bergerat, F., & Laurent, P. (1990). Polyphase tectonics and stress perturbations in the rhine-saone transform zone inferred from both analyses of calcite twins and fault slips. *Bulletin de la Societe Geologique de France, 6*, 853–863.

Lacombe, O., Angelier, J., Byrne, D., & Dupin, J. M. (1993). Eocene-Oligocene tectonics and kinematics of the Rhine-Saone Continental Transform Zone (eastern France). *Tectonics, 12*, 874–888. doi:10.1029/93TC00233.

Lacombe, O., & Mouthereau, F. (2002). Basement-involved shortening and deep detachment tectonics in forelands of orogens: Insights from recent collision belts (Taiwan, Western Alps, Pyrenees). *Tectonics, 21*, 12-1. doi:10.1029/2001TC901018.

Laubscher, H. (1992). Jura kinematics and the Molasse Basin. *Eclogae Geologicae Helvetiae, 85*, 653–675.

Laubscher, H. (2010). Jura, Alps and the boundary of the Adria subplate. *Tectonophysics, 483*, 223–239. doi:10.1016/j.tecto.2009.10.011.

Lebeau, R. (1951). Sur la structure du Jura: les enseignements de l'excursion géologique interuniversitaire en Franche-Comté (31 août–6 septembre 1949). *Revue de Géographie de Lyon, 26*, 71–75. doi:10.3406/geoca.1951.6039.

LeMasurier, W. E., & Landis, C. A. (1996). Mantle-plume activity recorded by low-relief erosion surfaces in West Antarctica and New Zealand. *Geological Society of America Bulletin, 108*, 1450–1466. doi:10.1130/0016-7606(1996)108<1450:MPARBL>2.3.CO;2.

Lippitsch, R., Kissling, E., & Ansorge, J. (2003). Upper mantle structure beneath the Alpine orogen from high-resolution

teleseismic tomography. *Journal of Geophysical Research: Solid Earth, 108*, 2376. doi:10.1029/2002JB002016.

Lyon-Caen, H., & Molnar, P. (1989). Constraints on the deep structure and dynamic processes beneath the Alps and adjacent regions from an analysis of gravity anomalies. *Geophysical Journal International, 99*, 19–32. doi:10.1111/j.1365-246X.1989.tb02013.x.

Madritsch, H. (2008). *Structural evolution and neotectonics of the Rhine-Bresse Transfert Zone*. Basel: University of Basel.

Madritsch, H., Fabbri, O., Hagedorn, E.-M., Preusser, F., Schmid, S. M., & Ziegler, P. A. (2010a). Feedback between erosion and active deformation: geomorphic constraints from the frontal Jura fold-and-thrust belt (eastern France). *International Journal of Earth Sciences, 99*, S103–S122. doi:10.1007/s00531-009-0468-7.

Madritsch, H., Kounov, A., Schmid, S. M., & Fabbri, O. (2009). Multiple fault reactivations within the intra-continental Rhine-Bresse Transfer Zone (La Serre Horst, eastern France). *Tectonophysics, 471*, 297–318. doi:10.1016/j.tecto.2009.02.044.

Madritsch, H., Preusser, F., & Fabbri, O. (2012). Climatic and tectonic controls on the development of the River Ognon terrace system (eastern France). *Geomorphology, 151*, 126–138. doi:10.1016/j.geomorph.2012.01.023.

Madritsch, H., Preusser, F., Fabbri, O., Bichet, V., Schlunegger, F., & Schmid, S. M. (2010b). Late Quaternary folding in the Jura Mountains: evidence from syn-erosional deformation of fluvial meanders. *Terra Nova, 22*, 147–154. doi:10.1111/j.1365-3121.2010.00928.x.

Merle, O., & Michon, L. (2001). The formation of the West European Rift; a new model as exemplified by the Massif Central area. *Bulletin de la Societe Geologique de France, 172*, 213–221. doi:10.2113/172.2.213.

Mocochain, L., Clauzon, G., Bigot, J.-Y., & Brunet, P. (2006). Geodynamic evolution of the peri-Mediterranean karst during the Messinian and the Pliocene: evidence from the Ardèche and Rhône Valley systems canyons, Southern France. *Sedimentary Geology, 188–189*, 219–233. doi:10.1016/j.sedgeo.2006.03.006.

Molliex, S., Fabbri, O., Bichet, V., & Madritsch, H. (2011). Possible Quaternary growth of a hidden anticline at the front of the Jura fold-and-thrust belt: geomorphological constraints from the Foret de Chaux area. *Bulletin de la Société Géologique de France, 182*, 337–346.

Molnar, P. (2009). The state of interactions among tectonics, erosion, and climate: A polemic. *GSA Today, 19*, 44–45. doi:10.1130/GSATG00GW.1.

Molnar, P., & England, P. (1990). Late Cenozoic uplift of mountain-ranges and global climate change—Chicken or egg. *Nature, 346*, 29–34. doi:10.1038/346029a0.

Monbaron, M. (1975). *Contribution à l'étude des cluses du jura septentrional (Thèse Universitaire)*. Neuchatel: Université de Neuchâtel.

Mosar, J. (1999). Present-day and future tectonic underplating in the western Swiss Alps: Reconciliation of basement/wrench-faulting and décollement folding of the Jura and Molasse basin in the Alpine foreland. *Earth and Planetary Science Letters, 173*, 143–155. doi:10.1016/S0012-821X(99)00238-1.

Mudry, J., & Rosenthal, P. (1977). *La Haute-chaîne du Jura entre Morez, Saint-Claude et la Pesse. Étude géologique et hydrologique*. Besançon: Université de Franche-Comté.

Nivière, B., Giamboni, M., Innocent, C., & Winter, T. (2006). Kinematic evolution of a tectonic wedge above a flat-lying décollement: The Alpine foreland at the interface between the Jura Mountains (Northern Alps) and the Upper Rhine graben. *Geology, 34*, 469–472. doi:10.1130/G22334.1.

Nivière, B., & Winter, T. (2000). Pleistocene northwards fold propagation of the Jura within the southern Upper Rhine Graben: Seismotectonic implications. *Global and Planetary Change, 27*, 263–288. doi:10.1016/S0921-8181(01)00070-4.

Nocquet, J.-M. (2012). Present-day kinematics of the Mediterranean: A comprehensive overview of GPS results. *Tectonophysics, 579*, 220–242. doi:10.1016/j.tecto.2012.03.037.

Nocquet, J.-M., & Calais, E. (2003). Crustal velocity field of western Europe from permanent GPS array solutions, 1996–2001. *Geophysical Journal International, 154*, 72–88. doi:10.1046/j.1365-246X.2003.01935.x.

Norton, K. P., & Hampel, A. (2010). Postglacial rebound promotes glacial re-advances—A case study from the European Alps. *Terra Nova, 22*, 297–302. doi:10.1111/j.1365-3121.2010.00946.x.

Ostermann, M., Sanders, D., & Kramers, J. (2006). 230 234 Th/U ages of calcite cements of the proglacial valley fills of Gamperdona and Bürs (Riss ice age, Vorarlberg, Austria): geological implications_-_. *Austrian Journal of Earth Sciences, 230*, 234.

Perrin, J., & Luetscher, M. (2008). Inference of the structure of karst conduits using quantitative tracer tests and geological information: example of the Swiss Jura. *Hydrogeology Journal, 16*, 951–967. doi:10.1007/s10040-008-0281-6.

Persaud, M., & Pfiffner, O. A. (2004). Active deformation in the eastern Swiss Alps: Post-glacial faults, seismicity and surface uplift. *Tectonophysics, 385*, 59–84. doi:10.1016/j.tecto.2004.04.020.

Pfiffner, O. A. (1990). kinematics and intrabed-strain in mesoscopically folded limestone layers-examples from the jura and the helvetic zone of the alps. *Eclogae Geologicae Helvetiae, 83*, 585–602.

Phillips, J. D., McCormack, S., Duan, J., Russo, J. P., Schumacher, A. M., Tripathi, G. N., et al. (2010). Origin and interpretation of knickpoints in the Big South Fork River basin, Kentucky-Tennessee. *Geomorphology, 114*, 188–198. doi:10.1016/j.geomorph.2009.06.023.

Preusser, F., & Schlüchter, C. (2004). Dates from an important early Late Pleistocene ice advance in the Aare valley, Switzerland. *Eclogae Geologicae Helvetiae, 97*, 245–253. doi:10.1007/s00015-004-1119-4.

Rantitsch, G., Pischinger, G., & Kurz, W. (2009). Stream profile analysis of the Koralm Range (Eastern Alps). *Swiss Journal of Geosciences, 102*, 31–41. doi:10.1007/s00015-009-1305-5.

Robl, J., Stüwe, K., & Hergarten, S. (2008). Channel profiles around Himalayan river anticlines: Constraints on their formation from digital elevation model analysis. *Tectonics,*. doi:10.1029/2007TC002215.

Rollier, L. (1903). Le plissement de la chaine du Jura. *Annales de Géographie, 12*, 403–410. doi:10.3406/geo.1903.6377.

Ruddiman, W. F., & Kutzbach, J. E. (1989). Forcing of late Cenozoic northern hemisphere climate by plateau uplift in southern Asia and the American west. *Journal of Geophysical Research: Atmospheres, 94*, 18409–18427. doi:10.1029/JD094iD15p18409.

Ruddiman, W. F., Raymo, M. E., Lamb, H. H., & Andrews, J. T. (1988). Northern hemisphere climate regimes during the past 3 Ma: possible tectonic connections [and discussion]. *Philosophical Transactions of the Royal Society B: Biological Sciences, 318*, 411–430. doi:10.1098/rstb.1988.0017.

Schlatter, A., Schneider, D., Geiger, A., & Kahle, H.-G. (2005). Recent vertical movements from precise levelling in the vicinity of the city of Basel, Switzerland. *International Journal of Earth Sciences, 94*, 507–514. doi:10.1007/s00531-004-0449-9.

Schlunegger, F., & Hinderer, M. (2003). Pleistocene/Holocene climate change, re-establishment of fluvial drainage network and increase in relief in the Swiss Alps. *Terra Nova, 15*, 88–95. doi:10.1046/j.1365-3121.2003.00469.x.

Schlunegger, F., Jordan, T. E., & Klaper, E. M. (1997). Controls of erosional denudation in the orogen on foreland basin evolution:

The Oligocene central Swiss Molasse Basin as an example. *Tectonics, 16*, 823–840. doi:10.1029/97TC01657.

Serpelloni, E., Faccenna, C., Spada, G., Dong, D., & Williams, S. D. P. (2013). Vertical GPS ground motion rates in the Euro-Mediterranean region: New evidence of velocity gradients at different spatial scales along the Nubia-Eurasia plate boundary. *Journal of Geophysical Research: Solid Earth, 118*, 6003–6024. doi:10.1002/2013JB010102.

Shahzad, F., Mahmood, S. A., & Gloaguen, R. (2007). *Stream profile and neotectonic analysis in Hazara Kashmir Syntaxis using shuttle radar digital elevation-data*. New York: IEEE.

Singh, T., & Awasthi, A. K. (2010). Stream profiles as indicator of active tectonic deformation along the Intra-Foreland Thrust, Nahan Salient, NW India. *Current Science, 98*, 95–98.

Smit, J. (2005), *Brittle-ductile coupling in thrust wedges and continental transforms*. Ph.D. thesis, Vrije Univ., Amsterdam, 115 pp.

Snyder, N. P., Whipple, K. X., Tucker, G. E., & Merritts, D. J. (2000). Landscape response to tectonic forcing: Digital elevation model analysis of stream profiles in the Mendocino triple junction region, northern California. *Geological Society of America Bulletin, 112*, 1250–1263. doi:10.1130/0016-7606(2000)112<1250:LRTTFD>2.0.CO;2.

Sommaruga, A. (1999). Decollement tectonics in the Jura foreland fold-and-thrust belt. *Marine and Petroleum Geology, 16*, 111–134. doi:10.1016/S0264-8172(98)00068-3.

Sougnez, N., & Vanacker, V. (2010). Spatial variability in channel and slope morphology within the Ardennes Massif, and its link with tectonics. *Hydrology and Earth System Sciences Discussions, 7*, 6981–7006.

Steer, P., Simoes, M., Cattin, R., & Shyu, J. B. H. (2014). Erosion influences the seismicity of active thrust faults. *Nature Communications,*. doi:10.1038/ncomms6564.

Sternai, P., Herman, F., Champagnac, J.-D., Fox, M., Salcher, B., & Willett, S. D. (2012). Pre-glacial topography of the European Alps. *Geology, 40*, 1067–1070. doi:10.1130/G33540.1.

Stocchi, P., & Spada, G. (2009). Influence of glacial isostatic adjustment upon current sea level variations in the Mediterranean. *Tectonophysics, TOPO-EUROPE: The Geoscience of coupled Deep Earth-surface processes, 474*, 56–68. doi:10.1016/j.tecto.2009.01.003.

Sue, C., Delacou, B., Champagnac, J.-D., Allanic, C., Tricart, P., & Burkhard, M. (2007). Extensional neotectonics around the bend of the Western/Central Alps: An overview. *International Journal of Earth Sciences, 96*, 1101–1129. doi:10.1007/s00531-007-0181-3.

Sue, C., Thouvenot, F., Frechet, J., & Tricart, P. (1999). Widespread extension in the core of the western Alps revealed by earthquake analysis. *Journal of Geophysical Research: Solid Earth, 104*, 25611–25622. doi:10.1029/1999JB900249.

Thomson, S. N., Brandon, M. T., Tomkin, J. H., Reiners, P. W., Vásquez, C., & Wilson, N. J. (2010). Glaciation as a destructive and constructive control on mountain building. *Nature, 467*, 313–317. doi:10.1038/nature09365.

Ustaszewski, K., & Schmid, S. M. (2006). Control of preexisting faults on geometry and kinematics in the northernmost part of the Jura fold-and-thrust belt. *Tectonics,*. doi:10.1029/2005TC001915.

Ustaszewski, K., & Schmid, S. M. (2007). Latest Pliocene to recent thick-skinned tectonics at the Upper Rhine Graben—Jura Mountains junction. *Swiss Journal of Geosciences, 100*, 293–312. doi:10.1007/s00015-007-1226-0.

Valla, P. G., Shuster, D. L., & van der Beek, P. A. (2011). Significant increase in relief of the European Alps during mid-Pleistocene glaciations. *Nature Geoscience, 4*, 688–692. doi:10.1038/ngeo1242.

Valla, P. G., van der Beek, P. A., Shuster, D. L., Braun, J., Herman, F., Tassan-Got, L., & Gautheron, C. (2012). Late Neogene exhumation and relief development of the Aar and Aiguilles Rouges massifs (Swiss Alps) from low-temperature thermochronology modeling and 4He/3He thermochronometry. *Journal of Geophysical Research: Earth Surface, 117*, F01004. doi:10.1029/2011JF002043.

Van der Beek, P., & Bourbon, P. (2008). A quantification of the glacial imprint on relief development in the French western Alps. *Geomorphology, Glacial Landscape Evolution—Implications for Glacial Processes, Patterns and Reconstructions, 97*, 52–72. doi:10.1016/j.geomorph.2007.02.038.

Vernant, P., Hivert, F., Chéry, J., Steer, P., Cattin, R., & Rigo, A. (2013). Erosion-induced isostatic rebound triggers extension in low convergent mountain ranges. *Geology, 41*, 467–470. doi:10.1130/G33942.1.

Walpersdorf, A., Baize, S., Calais, E., Tregoning, P., & Nocquet, J.-M. (2006). Deformation in the Jura Mountains (France): First results from semi-permanent GPS measurements. *Earth and Planetary Science Letters, 245*, 365–372. doi:10.1016/j.epsl.2006.02.037.

Whipple, K. X. (2001). Fluvial landscape response time: How plausible is steady-state denudation? *American Journal of Science, 301*, 313–325. doi:10.2475/ajs.301.4-5.313.

Whipple, K. X. (2004). Bedrock rivers and the geomorphology of active orogens. *Annual Review of Earth and Planetary Sciences, 32*, 151–185. doi:10.1146/annurev.earth.32.101802.120356.

Whipple, K. X. (2009). The influence of climate on the tectonic evolution of mountain belts (vol 2, pg 97, 2009). *Nature Geoscience, 2*, 730. doi:10.1038/ngeo638.

Whipple, K. X., & Tucker, G. E. (1999). Dynamics of the stream-power river incision model: Implications for height limits of mountain ranges, landscape response timescales, and research needs. *Journal of Geophysical Research: Solid Earth, 104*, 17661–17674. doi:10.1029/1999JB900120.

Whipple, K., Wobus, C., Crosby, B., Kirby, E., & Sheehan, D. (2007). New tools for quantitative geomorphology: extraction and interpretation of stream profiles from digital topographic data, online report. GSA Annual Meetimg. http://www.geomorphtools.org/Tools/StPro/Tutorials/StPro_UserGuidees_Final.pdf.

Willett, S. D., McCoy, S. W., Perron, J. T., Goren, L., & Chen, C.-Y. (2014). Dynamic reorganization of river basins. *Science, 343*, 1248765. doi:10.1126/science.1248765.

Willgoose, G., Bras, R. L., & Rodriguez-Iturbe, I. (1991a). A coupled channel network growth and hillslope evolution model: 1 Theory. *Water Resources Research, 27*, 1671–1684. doi:10.1029/91WR00935.

Willgoose, G., Bras, R. L., & Rodriguez-Iturbe, I. (1991b). A coupled channel network growth and hillslope evolution model: 2 Nondimensionalization and applications. *Water Resources Research, 27*, 1685–1696. doi:10.1029/91WR00936.

Wobus, C., Whipple, K. X., Kirby, E., Snyder, N., Johnson, J., Spyropolou, K., et al. (2006). Tectonics from topography: Procedures, promise, and pitfalls. *Geological Society of America Special Paper, 398*, 55–74. doi:10.1130/2006.2398(04).

Walsh, L. S., Martin, A. J., Ojha, T. P., & Fedenczuk, T. (2012). Correlations of fluvial knickzones with landslide dams, lithologic contacts, and faults in the southwestern Annapurna Range, central Nepalese Himalaya. *Journal of Geophysical Research: Earth Surface,*. doi:10.1029/2011JF001984.

Yanites, B. J., Ehlers, T. A., Becker, J. K., Schnellmann, M., & Heuberger, S. (2013). High magnitude and rapid incision from river capture: Rhine River, Switzerland. *Journal of Geophysical Research: Earth Surface, 118*, 1060–1084. doi:10.1002/jgrf.20056.

Ziegler, P. A., & Fraefel, M. (2009). Response of drainage systems to Neogene evolution of the Jura fold-thrust belt and Upper Rhine Graben. *Swiss Journal of Geosciences, 102*, 57–75. doi:10.1007/s00015-009-1306-4.